Correlating the development of chloride profiles and microstructural changes in marine concrete up to ten years

Simon Fjendbo [a,b,*], Henrik E. Sørensen [a], Klaartje De Weerdt [b], Ulla H. Jakobsen [a], Mette R. Geiker [b]

[a] *Danish Technological Institute, Taastrup, Denmark*
[b] *Norwegian University of Science and Technology (NTNU), Department of Structural Engineering, Trondheim, Norway*

A R T I C L E   I N F O

A B S T R A C T

After ten years of marine exposure, chloride and calcium profiles and petrographic data were obtained from the tidal and submerged zones of six concrete panels differing in binder composition. Moisture and portlandite profiles were also determined on the submerged concrete. The data enables us to improve our understanding of the impact of sea water exposure and can also be used for service life modeling.

The depth of the maximum chloride content and the depth of the microstructurally changed zone were comparable. Both depths progressed over time and reached a depth of as much as 10 mm after ten years of exposure.

When using these and other field data for testing of chloride ingress prediction models, we recommend excluding datapoints from the microstructurally changed zone, i.e., the outermost datapoints including the maximum chloride content, unless reactive transport models are used.

1. Introduction

Chloride ingress profiles are often used for the design and residual service life assessment of reinforced concrete structures susceptible to reinforcement corrosion. In 2010, Femern A/S established a field exposure station in Rødbyhavn, Denmark, as part of the preparatory work for the upcoming Fehmarn Belt fixed link between Denmark and Germany. The purpose was to support the design and operation of the reinforced concrete structures for the fixed link. Chloride profiles taken from concrete subject to tidal and submerged exposure for five years at the Fehmarn Belt Exposure Site [1] and petrographic analysis of concrete subject to five years' tidal exposure [2] have already been reported. Recently, chloride ingress data from several exposure sites, including the Fehmarn Belt Exposure Site, have been compiled and analyzed using a square root of exposure time vs. chloride ingress depth approach [3].

Multiple factors influence chloride ingress in concrete [4–21]. In partly saturated concrete, chloride can enter both by capillary suction and by diffusion. The rate of diffusion depends on the concentration difference and the diffusion coefficient, which increases with increasing moisture content [5–9]. Nielsen and Geiker [6] proposed an approach

based on Powers' model for deriving the dependency of the chloride diffusion coefficient on the degree of saturation of the capillary porosity. Olsson et al. [7] concluded that there is a clear relationship between the calculated diffusion coefficient and the moisture content for individual binders based on experiments that showed an exponential increase in the relative diffusion coefficient with an increasing degree of saturation. Concrete in the marine splash and tidal zone will suffer chloride ingress by capillary suction of sea water in the convection zone and chloride ingress by diffusion at greater depths. During drying, chlorides will accumulate at the evaporation front, which could lead to an expectation that at early ages the rate of chloride ingress would be faster in concrete exposed to wetting and drying due to a higher surface concentration, whereas at later ages the concrete with highest moisture content might suffer deeper ingress due to a higher diffusion coefficient. Geiker [22] gives examples of chloride ingress in marine concrete, and Jensen et al. [23] have calculated the apparent chloride diffusion coefficient and surface concentration using the error function solution to Fick's second law and omitting surface near data points where reduced chloride content was measured based on the chloride profiles from submerged exposure and level 0.35, 0.5, 0.7–0.9 and 1.5 m above mean water level. In general, they found that a) the highest diffusion coefficients and

---

Table 1
Concrete compositions[kg/m3] [1].

ID used in this paper		PC	15FA	25FA	4SF	12FA4SF	SG
Original concrete ID [44]		A	B	C	E	F	K
Powder composition [% by wt.]	CEM I	100	85	75	96	84	
	FA[a]		15	25		12	
	SF[b]				4	4	
	CEM III						100
CEM I 42.5 N-SR5[c]		360	319	298	340	297	
CEM III/B 42.5 N[c,d]							359
FA [a]			56	99		42	
SF [b]					14	14	
Water		146	140	140	147	140	144
Superplasticizer 1[e]			2.3	2.2			
Superplasticizer 2[f]		2.7			2.6	2.9	2.4
Air entraining agent		1.7	1.7	2.2	0.6	1.5	0.8
Sand (0–2 mm)		686	655	630	693	670	687
Coarse aggregates (4–22 mm)		1155	1182	1170	1167	1192	1157
w/b[g]		0.40	0.37	0.35	0.42	0.40	0.40
w/(c + 2SF + 0.5 FA)		0.40	0.40	0.40	0.40	0.40	0.40
Density [kg/m³]		2346	2345	2329	2349	2346	2320
Air [% by vol.]		5.8	5.4	5.5	4.8	5.2	4.4

[a] FA = Fly ash.
[b] SF = Silica fume (dry matter), (added as slurry).
[c] According to EN 197-1.
[d] SG = Ground Granulated Blast-furnace Slag (GGBS) content: 67% by wt.
[e] BASF Glenium SKY 532 S (Polycarboxylate ether).
[f] BASF Glenium SKY 540 (Polycarboxylate ether).
[g] w = Water. b = CEM (I or III) + SF + FA.

medium surface concentrations were in the submerged zone, and b) the highest surface concentrations and medium diffusion coefficients were in the lower part of the splash zone.

Multiple ions in sea water, such as magnesium, sulfate and carbonate ions, combined with the leaching of calcium, potassium and hydroxyl ions can influence chloride ingress by altering the microstructural properties and the binding capacity of the paste, and they can change the porosity in the outer surface and even cause surface scaling [10–14]. For marine-exposed concretes, elemental zonation has been observed as a general feature, consisting of a magnesium-enriched zone near the surface, followed by a sulfur-enriched zone, and finally a chloride-enriched zone [10,15]. This explains why the chloride concentration is not highest at the surface, both in cases with convection zones and also in submerged exposure [10].

Depending on the difference in composition and concentrations of ions in sea water and in the concrete pore solution, some ions ingress while others are leached out. Typically the ions mentioned in the previous paragraph ingress, while the portlandite leach out and calcium-silicon ratio of the C–S–H gel decreased with increased exposure time [16]. De Weerdt et al. [19] showed that, for long-term marine-exposed concrete, the depth of portlandite leaching might be comparable to the depth of chloride ingress. A well-known consequence of leaching is an increase in porosity and a potential decrease in mechanical strength [17]. However, what seems less recognized is that leaching also affects the chloride binding capacity, initially causing an increase, but later a decrease.

Chloride in concrete can be found free in the pore solution, physically bound (adsorbed) in calcium silicate hydrate (C–S–H), or chemically bound in chloride-containing AFms like Friedel's or Kuzel's salt [17]. Hemstad et al. [18] found that the pH of the pore solution influences the chloride binding capacity in Portland cement pastes. Lowering the pH from 13 to 12 increased chloride binding, which was associated with increased chloride binding in the AFm phases and potentially also the C–S–H. However, lowering the pH below 12 reduced chloride binding, partly due to the dissolution of AFms and most likely a reduction in the adsorption of chlorides by C–S–H [18,24]. The intermediate step with increased chloride binding explains the observed gradually inwards-moving maximum chloride content [18]. Machner

et al. [25] recently demonstrated that leaching has a profound impact on the chloride ingress profiles and briefly discussed implications for both performance testing and service life prediction.

Sulfate is expected to reduce chloride binding because sulfates compete with chlorides for incorporation in C–S–H and calcium aluminate phases [20]. Sulfate ions in concrete can react to form gypsum, ettringite and thaumasite. Typically, gypsum is formed near the surface [2], and ettringite and thaumasite are found slightly deeper in Ref. [17]. The formation of ettringite and thaumasite typically leads to a significant volume increase which could result in cracking [26], but when they form in the large voids in the sulfur-rich zone of marine-exposed concrete, cracking is limited or absent [10,27].

Magnesium originating from sea water can precipitate as brucite when it encounters the high pH of the concrete [28] or as the non-cementing magnesium silicate hydrate (M-S-H) [21,29]. M-S-H replaces C–S–H, which leads to a reduction in the chloride binding [10, 21]. It has also been reported to result in a weak, cracked and porous zone [10], which might be absent in field samples due to abrasion [13, 17].

The precipitation of a surface layer of brucite and/or calcite on the concrete and the formation of ettringite in the near-surface region due to the presence of magnesium, carbonate or sulfate ions from the sea water [30] have not been observed to limit chloride ingress in concrete [10, 31].

For design and reassessment purposes, the error function solution to Fick's 2nd law of diffusion is often used for chloride ingress prediction [32–36]. Among other things, this use is based on the assumptions that concrete is a homogeneous material and that no reactions occur between solids and the diffusing species [37]. These assumptions are questionable not only due to variations in the initial material, but also due to the multitude of reactions occurring over time in the surface of concrete exposed to sea water, as discussed above [10,12,13,16–21,26–29,31,38, 39]. There are various views on how to overcome this challenge [36,40].

For design purposes, *fib* [36] proposes a so-called transfer function Δx, which is to be added to the calculated ingress depth for splash and tidal exposures to account for rapid chloride ingress (by convection) down to a given depth, but not for submerged exposure [36]. Similarly, Toutlemonde et al. [41] propose a so-called convection depth (Δx) for

Table 2

Chemical composition and physical properties of binders. The chemical composition was measured by X-ray fluorescence according to EN 196-2. "-" means that the amount has not been measured.

Property		CEM I [% by wt.]	FA [% by wt.]	SF [% by wt.]	CEM III [% by wt.]
Oxide	Al_2O_3	2.91	20.5	–	9.44
	SiO_2	24.8	60.3	95.4	30.5
	CaO	65.6	1.56	0.32	47.8
	CO_2	0.15	–	–	0.75
	Cl^-	0.00	0.01	0.04	0.08
	Fe_2O_3	2.34	7.39	–	0.74
	MgO	0.75	–	–	4.88
	SO_3	2.24	0.46	0.23	2.54
	Na_2O_{eq}	0.40	2.76	0.72	0.78
	Na_2O	–	–	0.19[1]	0.33[1]
	K_2O	–	–	0.80[1]	0.48[1]
Loss on ignition		0.65	3.17	1.34	1.05
Blaine surface [m^2/kg]		366	–	23740	487
Density [kg/m^3]		3190	2348	–	2961
Fineness (wt% passing 0.045 mm sieve)		–	84	–	–

1) Value declared by producer in a technical data sheet.
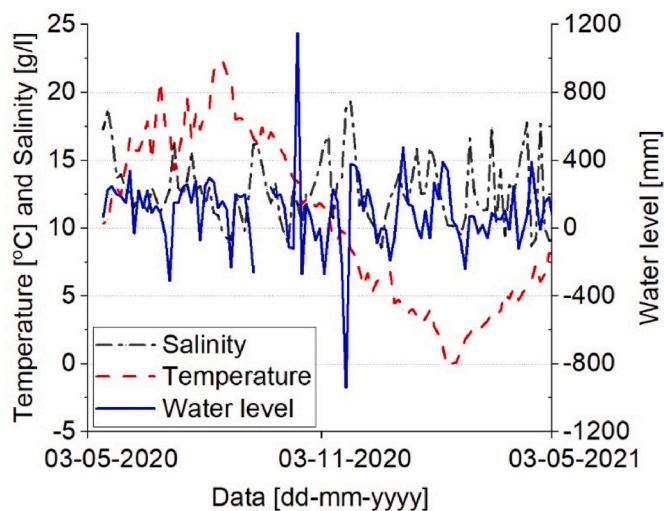
Fig. 1. Exposure conditions: water temperature, salinity, and water level (one year).

Table 3

Exposure conditions (average of one year using data from Fig. 1).

Average temperature (atmosphere) [°C]	11.2 (monthly min.: 2.1, monthly max.: 18.2)
Average temperature (sea water) [°C]	10.5 (min.: 0.3, max.: 22.4)
Average salinity (sea water) [g/l]	12.7 (min.: 8.6, max.: 19.3)
Average chloride content (sea water) [g/l]	7.0[a] (min.: 4.7, max.: 10.6)

a) Assuming a distribution of ions in the sea water as in the Baltic Sea [46].

beyond the concrete surface. They propose that the fitting should be performed on a rescaled profile where the origin is moved to x_{Cmax} [40]. When later predicting chloride ingress, x_{Cmax} is to be added to the predicted chloride ingress depth [40]. This approach corresponds to the assumption of the non-Fickian behavior observed in the outer surface is caused by rapid ingress by convection applied in the *fib* Model Code for Service Life Design. Andrade et al. [40] further note that in cases where the value and position of the maximum chloride content progress, the controlling mechanisms have not yet been identified. In these cases, they recommend not making a prediction without emphasizing its limitations [40]. This paper investigates the relationship between chloride profiles and the development of a microstructurally changed zone. The investigation covers chloride profiles combined with petrographic analysis of tidal and submerged concrete after ten years of marine exposure, supplemented with moisture and portlandite profiles of the submerged exposed concrete and earlier data on microstructure and chloride ingress.

The main findings are a gradually progressing microstructurally changed zone correlating with the observed peaking behavior of chloride profiles in submerged marine exposed concrete. After 10 years exposure, the comparable depth of the maximum chloride content and the depth of the microstructurally changed zone had a non-negligible depth of 10 mm.

Based on the experimental data, we recommend that only data unaffected by the microstructural changes should be applied for service life predictions unless reactive transport models are used.

2. Experimental

2.1. Materials

We investigated cores from six out of 15 unreinforced concrete panels subjected to marine exposure for ten years at the Fehmarn Belt Exposure Site, Rødbyhavn, Denmark.

2.1.1. Concrete panels, composition, and production

Table 1 gives an overview of the mixture proportions of the six different concretes analyzed, along with the IDs used in this paper. All cement notations are according to EN 197-1 [42]. Table 2 gives information on the chemical composition of binders as measured by X-ray fluorescence according to EN 196-2 [43].

Following the experience of two-sided ingress in some 0.1 m thick concrete panels exposed at Träslövsläge Field Exposure Site, it was decided to produce the panels for the Fehmarn Belt Exposure Site with a thickness of 0.2 m to considerably delay the time when two-sided ingress would occur. The concrete for the panels was produced in 0.230 m^3 batches and mixed in the Danish Technological Institute's Haarup counterflow mixer with a capacity of 0.250 m^3. Two batches were required for each concrete panel, and they were therefore transferred to and homogenized in a 0.540 m^3 pan mixer. After homogenization, the concrete panels were cast by filling from the top of the formwork (plywood, dimensions 2.0 m height, 1.0 m width, 0.2 m thickness) at a maximum drop height of 2.2 m. The concrete was cast in five layers, each of which was compacted using a small poker vibrator. Due to the wall effect (restricted aggregate packing in the outermost zone), there was a higher paste content in the outer section than in the bulk. Calcium profiles measured after six months give a rough impression of the magnitude of the wall effect, see Appendix A.

Maturity gain was monitored using embedded temperature sensors. Demolding was performed at a maturity of at least 24 h. After demolding, the panels were wrapped in plastic and stored indoors (approx. 20 °C) for at least 14 maturity days. The concretes were produced over a period of two months but exposed to the marine environment at the same time. To obtain similar maturity (approximately 45 days) at exposure, some panels were moved to a lower temperature (minimum 5 °C) for part of the curing period.

splash and tidal but not submerged exposures in a draft of a background document for the revision of EN1992, in which they also propose the use of a slightly greater convection depth for a design service life of 100 years than for 50 years (10 vs. 8 mm). For the assessment of chloride profiles where neither the maximum chloride content (C_{max}) nor its position (x_{Cmax}) are time-dependent, Andrade et al. [40] propose that the external layer showing an increase in chloride content with depth should be neglected when fitting a chloride profile with a maximum

Fig. 2. Location of cores extracted after ten years of exposure. The pattern covering positions #2 and #8 indicates that they were not cleaned prior to coring. Vertical distances from core center to bottom of the panel are shown in Table 4. All measures are in mm. "low" and "high" sea level are the 5th and 95th percentiles of the water level.

2.1.2. Exposure

Knowledge of the exposure environment is important because the condition of a concrete after a given exposure time is a result of the environment to which it has been exposed. The six concrete panels were exposed to sea water at the exposure site at a maturity of 43–49 days [44]. Fig. 1 shows the variation in temperature and salinity of the sea water and the water level over one year. Table 3 shows annual averages, including air temperature, using sensors installed by the Danish Hydraulic Institute. The panels were exposed partly submerged with 0.7 m of the 2.0 m high panels located above mean water level. Note that the recorded chloride content (7 g/l) is considerably less than the chloride content of the Atlantic Ocean (19 g/l), but the ratio between ions is similar [10,45].

2.1.3. Sample extraction

After ten years of exposure, the concrete panels were extracted from the sea water and brought to the laboratory at the Danish Technological Institute, and seven Ø100 mm cores were drilled from each concrete panel.

The positions of the cores investigated in this study and the notations used are shown in Fig. 2. Appendix B shows the entire sampling plan made during the design of the elements (more than ten years ago). Table 4 gives an overview of the cores investigated in this study: their position, exposure, orientation, investigated properties, and methods applied. The cores were drilled through the panels. The orientation west (W) and east (E) refers to the orientation faced by the analyzed surfaces. The panels are attached perpendicular to the quay. The short side of the panels nearest to the quay is facing north. The prevailing wind is coming from west, but the panels are mounted with a short distance of 20 cm to each other, and no significant differences are expected based on orientation. The subdivision of the cores is described in more detail in the following method descriptions. The numbering of the cores in Fig. 2 and Table 4 does not include 6 or 7, because no core was extracted at these core positions (In Appendix B these are marked as "Extra" as cores can be drilled here at later exposure times).

Before coring, organic growth was scraped off to allow space for the drilling equipment and limit bad odor during processing, except for the horizontal bands where cores #2 and #8 are positioned (see Fig. 2); they were not cleaned prior to core drilling because a fully intact surface was desired for petrographic analysis.

Right after coring, each core was cleaned by dipping it in a bucket of tap water and wiping the surface dry with a moist cloth and wrapped in plastic. All cores were stored sealed in plastic bags at 5 °C, except for cores #2 and #8 which were immediately processed for moisture and porosity determination and/or impregnated with epoxy in preparation for petrography as described in Sections 2.1.4, 2.2.3 and 2.2.7.

The abbreviations used to refer to the cores (or samples) are based on the concrete composition and, in the case of chloride ingress and petrography results only, the exposure condition (Tidal or Submerged) and the direction of the exposed surface (East or West). E.g., 12FA4SF-S-W stands for a concrete, which contains 12% fly ash and 4% silica fume, submerged exposure and west-facing surface, also referred to simply as 12FA4SF.

Table 4

Overview of cores: position (distance from bottom of element), exposure zone, orientation, property measured, and methods applied.

Core # (vertical position)	Position, mm from Bottom	Exposure zone	Orientation (E = east; W = west)	Property measured	Comment
9	1325	Tidal	W, E	Chloride and calcium profiles	See Section 2.2.5
8	1175	Tidal	W, E	Microstructure and air void structure	See Section 2.2.3 Three thin sections per core (two surfaces and one center)
			W	Elemental analysis	See Section 2.2.4 One polished section from SG
5	725	Submerged		Compressive strength	See Section 2.2.2
4	575	Submerged			
3	425	Submerged			
2	275	Submerged	W	Degree of capillary saturation, RH, total porosity, moisture profile	See Section 2.2.7
			W	Microstructure and air void structure	See Section 2.2.3. One thin section per core (west-facing surface)
1	125	Submerged	W, E	Chloride and calcium profiles	See Section 2.2.5
			W	Portlandite profiles	See Section 2.2.6
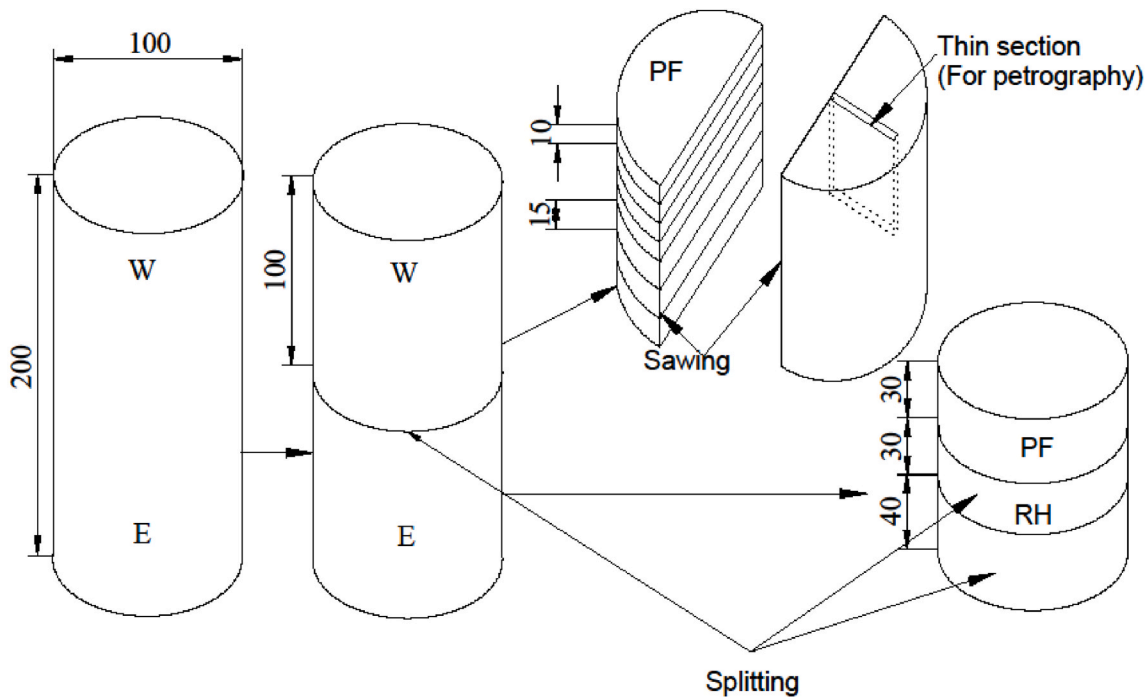
Fig. 3. Subdivision of #2 cores. Position of samples for determination of relative humidity (RH) as well as degree of capillary saturation (DCS) and porosity (marked "PF", see method description in 2.2.7). All measures are in mm. W: west-facing, E: east-facing.

2.1.4. Subdivision of cores

The #1 and #9 cores were cut off at a depth corresponding to the estimated ingress depth +15 mm to ensure that they retained material sufficiently deep to obtain the background chloride level. The chloride ingress depth after ten years of exposure was estimated by the square root method based on chloride ingress data after half a year, two, or five years of exposure [3]. The cores were further treated as described in Section 2.2.5.

The #2 cores were subdivided as shown in Fig. 3. To limit moisture redistribution and drying, the pieces were subdivided immediately after core drilling. Several scales were drawn on the cores to keep track of the actual splitting depths. The cores were first split into two approximately equal-sized half-cores. One half (east-facing) was further split into slices and used for determining (i) the degree of capillary saturation (DCS) and porosity using a modified version of the so-called "pore protection factor method" (PF), and (ii) the relative humidity (RH) of the "bulk", whereas the other half (west-facing) was used for measuring DCS and porosity profiles in sawn discs. The (east-facing) half cores used for "bulk" DCS, porosity and RH were split so the sample for DCS and porosity determination was positioned closest to the split surface and the sample for RH next to it, as shown in Fig. 3. The slices labeled PF and RH were further processed as described in Section 2.2.7. The other (west-facing) half core used for moisture profiles and petrography was sawn using a water-cooled mechanical saw. First, the coarse surface originating from splitting was sawn off. Then the half-cores were divided axially in half, and one of these half cylinders was subdivided inwards from the exposed surface into seven slices, where the four outermost slices were 10 mm thick, the next two were 15 mm thick, and the last slice was approximately 10 mm. Immediately after being sawn, the slices were dipped in water, wiped surface-dry with a moist cloth and weighed. Then the sample heights were measured, and their actual position in the panel calculated assuming equal loss due to sawing between each slice. From the second half cylinder of the west-facing part, a thin section was prepared for petrography (see Fig. 3).

The #3, #4 and #5 cores were ground clean on the surface using a grinding cup to achieve a specimen flatness conforming with DS/EN 12390–1:2000 [47] and used for testing of compressive strength

(dimensions approx. Ø100 × 196 mm).

Three thin sections were prepared from the #8 cores using the technique described by Jakobsen et al. [48]. One at a similar position at the west-facing surface as shown in Fig. 3 and an additionally one at the east-facing surface, and one in the center of the cores.

2.2. Methods

2.2.1. Visual inspection

The concrete panels were visually inspected after being lifted out of the water and again after scraping off organic matter from parts of the panels. The panels were examined for organic growth, scaling, cracks, and mechanical damage originating from handling.

2.2.2. Determination of mechanical properties

Compressive strength was measured on #3, #4 and #5 cores in accordance with DS/EN 12390-3 [49]. Density was measured in accordance with DS/EN 12390–7:2012 [50].

2.2.3. Petrography

The petrographic examination was performed on fluorescent-impregnated thin sections from the #2 and #8 cores using a Leica DM2500P optical polarizing microscope equipped with a fluorescent facility. Each section was vacuum impregnated with an epoxy resin containing a fluorescent dye. Next, the impregnated section was mounted on a glass plate, and ground to a thickness of 20 μm. Finally, the section was covered by a cover glass. The thin section was then examined in a polarizing optical microscope using transmitted light, crossed polarized light, and blue transmitted light through a BG12 excitation filter with a K530 yellow blocking filter (fluorescent mode).

The vacuum impregnation of the section with epoxy fills all voids and cavities with fluorescent epoxy. When fluorescent light is transmitted through the thin section in the microscope, the fluorescent epoxy emits yellow light that makes voids, cavities, and cracks easy to identify. The fluorescent epoxy also impregnates the capillary pores in the hardened cement paste, which makes a dense cement paste with low capillary porosity appear a darker green than a more porous cement

Fig. 4. Visual appearance of an entire concrete panel right after lifting out of the water. The part below mean sea level (red line, 1.3 m from the bottom) is covered with barnacles and mussels, the upper approx. 0.35 m is dry, and in between is a gradual transition from heavy to light organic growth. (For interpretation of the references to colour in this figure legend, the reader is referred to the Web version of this article.)

Table 5
Compressive strength [MPa] of cores extracted after ten years of exposure.

Concrete ID	PC	15FA	25FA	4SF	12FA4SF	SG
#3 cores	64.8	76.4	76.2	76.5	73.9	67.0
#4 cores	65.4	76.6	74.2	79.1	78.2	67.2
#5 cores	64.3	79.0	73.6	75.6	73.1	65.4
Average	64.9	77.3	74.7	77.1	75.1	66.5
Standard	+/-	+/-	+/-	+/-	+/- 2.2	+/-
deviation	0.6	1.2	1.1	1.5		0.8

paste with a high capillary porosity.

The water-to-cement ratio (*w/c*) of the concrete was estimated with an accuracy of ±0.02 by comparing with known *w/c* references [48].

The thin sections were analyzed for scaling, carbonation, leaching, micro-cracks, capillary porosity, and re-precipitation of solids. Cracks were divided into three types, depending on the crack width: 1) Coarse cracks: > 100 μm; 2) Fine cracks: 10–100 μm; 3) Microcracks: < 10 μm.

2.2.4. Elemental analysis

As identification of some phases by petrography in the very dense slag containing concrete (SG) after 10 years exposure proved difficult due to a highly dense texture, a polished section was prepared for SEM from #2 core of SG. The polished section was placed next to the thin section and examined in a FEI Quanta 400 ESEM equipped with a

Thermo SNN EDS analysis unit operated in high vacuum mode at an accelerating voltage of 20 keV. The samples were analyzed for the elements: Na, Mg, Al, Si, S, P, Cl, K, Ca, Mn, Ti and Fe. Results were obtained by performing line traverses from the surface to a depth of 85–105 mm in selected paste areas measuring 10×10 μm. The analysis step size was 20 μm in the outer 100 μm, followed by steps of 100 μm up to 1 mm depth, then 0.25–0.5 mm up to 4 mm depth, 1 mm up to 10 mm depth, 2 mm up to 20 mm depth, and then finally 10 mm for the rest of the depth. Cement grains and aggregate were selectively avoided in the area selection.

2.2.5. Determination of chloride and calcium content

The #1 and #9 cores (see Fig. 2) were divided into 10–12 sections spanning over the estimated ingress depth with lowest depth increments near the surface. Sections up to 4 mm depth were profile-ground, whereas sections of 6–15 mm were cut using a water-cooled precision diamond saw and subsequently crushed.

Approx. 5 g of the concrete powder of each section was weighed after drying at 105 °C overnight. The dried powder was dissolved in 50 ml 75 °C warm (1:10) HNO_3 and left to digest overnight. The samples were filtrated the following day. After the initial filtration, the filter was washed twice with 1% HNO_3 and the container with the filtrate was filled up to 100 ml by adding demineralized water. The filtrate was used for both chloride and parallel calcium analyses to ensure comparable results.

For chloride analysis, 50 ml of filtrate was added to 50 ml demineralized water.

For calcium analysis 5 ml of filtrate was added to 90 ml demineralized water, 5 ml Triethylamine, 5 ml 5.0 M NaOH, and 0.15 g calcein indicator.

The chloride and calcium contents were measured using potentiometric titration with a TitroLine 7000 titrator from SI Analytics. The chemicals used for titration were 0.1 M $AgNO_3$ for chloride and 0.1 M EDTA disodium salt for calcium analysis.

The chloride profiles presented in the paper are total chloride content and not calibrated for calcium content.

For completeness calcium calibrated chloride profiles are shown in Appendix C. The equation used to calibrate for paste fraction is given in Eq. (1).

$$Cl_{calibrated} = \frac{wt\%Cl_{measured}}{wt\%CaO_{measured} \times \frac{40}{56}} \times wt\%Ca_{Theoretical} \qquad (1)$$

where Ca$_{Theoretical}$ is calculated based on the binder content of the concrete (Table 1) and the calcium content of the binders as measured by X-ray Fluorescence (Table 2). The molar weight of calcium is 40 g/mol, and 56 g/mol is the molar weight of calcium oxide. The calibration for the calcium content was originally done to correct for potential variations in the paste fraction, e.g., due to the wall effect. However, as discussed in a separate paper [51], leaching reduces the calcium content in the concrete, which is therefore not a stable measure for the paste fraction.

2.2.6. Determination of portlandite

To quantify the degree of leaching in the samples, portlandite (CH) profiles were obtained using a Mettler Toledo TGA/DSC 3+. Approximately 300 mg of the profile-ground powder from each section from #1 cores were loaded in 600 μl corundum crucibles. The samples were heated from 60 to 850 °C at a rate of 10 °C/min while using N_2 as purge gas at a flow of 50 mL/min. The mass loss of the samples was monitored as a function of temperature.

The mass loss due to CH decomposition was quantified by using the tangential method in the range 400–500 °C [52,53]. The limits of the temperature interval are determined based on the derivative of the mass loss curve. The CH content by wt.% of concrete was normalized to the dry sample weight at 850 °C in accordance with Eq. (2).
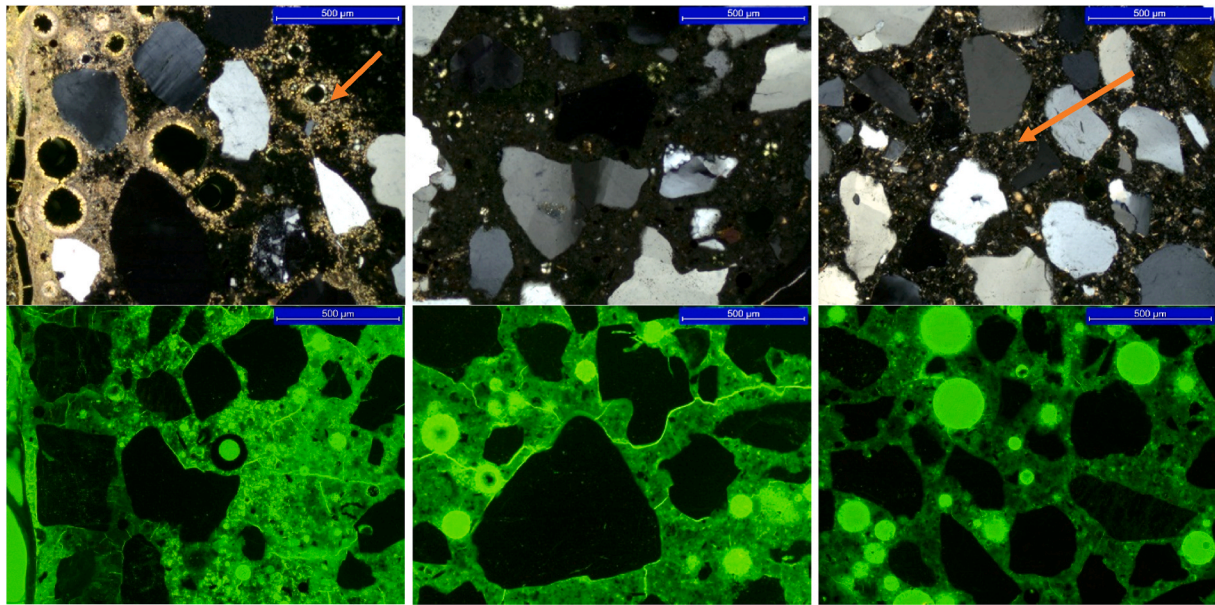
Surface zone (Typical <1 mm depth): intermixed leached paste and popcorn carbonation (marked with arrow), high porosity.

Opaline zone (Typical of 2–10 mm depth): no visible CH, with increased porosity and micro-cracking.

Bulk (Typical of >10 mm depth): visible CH (marked with arrow) and apparent *w/c* of 0.40.

Fig. 5. An example (concrete 15FA) of the microstructural change appearing in the surface region after ten years of submerged exposure to sea water (core #2; exposed surface is to the left). Images were taken in cross-polarized (top row) and fluorescent-light mode (bottom row) and measure 1.5 mm in width. The scale bar = 500 μm. The microstructurally changed zone includes: (left column) a slightly scaled surface zone with intermixed leached and popcorn-carbonated paste and high porosity; (center column) an opaline zone with a blurred appearance and no visible portlandite (CH), but often with ettringite and/or thaumasite in air voids; and (right column) bulk concrete with visible CH and an apparent w/c ratio of 0.40.

Table 6
Depths of various microstructurally changed zones, precipitated phases, and micro-cracks observed in the optical polarizing microscope after ten years of exposure (west-facing surface). Note that the depth of the zones was measured from the current surface and differs from the depth from the initial surface due to scaling.

Concrete ID		PC		15FA		25FA		4SF		12FA4SF		SG	
Submerged (S) or tidal (T)		T	S	T	S	T	S	T	S	T	S	T	S
Microstructurally changed zone	Black leached zone [mm]	1.2	0.3	0.4	0.3	0.2	0.8	0.2	0.3	0.6	0.4	0.4	0.4
	Zone with popcorn carbonation [mm]	2.0	1.2	1.2	1.6	1.0	1.2	1.2	1.2	2.0	1.2	2.0	3.0
	Opaline zone [mm]	10	10	7	10	10	10	8	8	7	10	_[d]	_[d]
	Porous zone [mm]	5	10	4	10	3	10	4	8	5	10	3	4
Excess ettringite in voids [mm]		8	10	10	6	6	11	6	9	10	6.5	13	10
Thaumasite in voids [mm]		4	4[a]	2	3	3	4[b]	3	3[c]	3	3	–	–
Depth with increased # of micro-cracks [mm]		10	10	8	10	6	9	15	8	20	10	12	5
Self-healing micro-cracks in outer max 2 mm		x	x	x	x	x	x	x	x	x	x	x	x

[a] Significant until 1.2 mm.

[b] Where surface is scaled. Only around 0.5 where surface is intact.

[c] Very systematic starting directly below the "popcorn-carbonated" zone down to about 1.5 mm below it, but locally found down to 4 mm, coinciding with the maximum depth of "popcorn" carbonation.

[d] Not seen for GGBS-based concrete.

$$CH = \frac{w_{400} - w_{500}}{w_{850}} \times \frac{74}{18} \qquad (2)$$

where w_{400}, w_{500} and w_{800} are the sample weights at approx. 400, 500 and 850 °C respectively, 74 g/mol is the molar weight of Ca(OH)$_2$, and 18 g/mol is the molar weight of H$_2$O.

2.2.7. Determination of moisture content and porosity

The moisture content was characterized as relative humidity (RH) and degree of capillary saturation (DCS). Porosity was determined as suction porosity relative to either drying at 50 °C or 105 °C, and macro porosity.

After subdivision as described in Section 2.1.4, the saw-cut concrete slices from the west-facing half #2 cores (labeled PF in Fig. 3) were immediately cleaned by dipping in a bucket of water, dried with a moist cloth, and weighed (w_{start}). The split slice from the east-facing half #2 cores were used directly. The timeframe from core drilling to measuring w_{start} was approximately 10 min. Each slice was subsequently partly submerged in a water bath for one day to avoid trapping of air, and thereafter fully submerged until it reached a constant mass (<0.02% weight change/day). The capillary-saturated slices were weighed in air (w_{sata}) and under water (w_{satw}) to determine their volume ($V = w_{sata}-w_{satw}$).

RH was determined on the slice labeled RH in Fig. 3. Initially, the edges were chiseled off to obtain a sample unaffected by drilling and potential immediate moisture loss. The sample was then crushed in a jaw crusher, and the finest parts most susceptible to moisture loss were quickly discarded through a 2 mm sieve, while the larger pieces
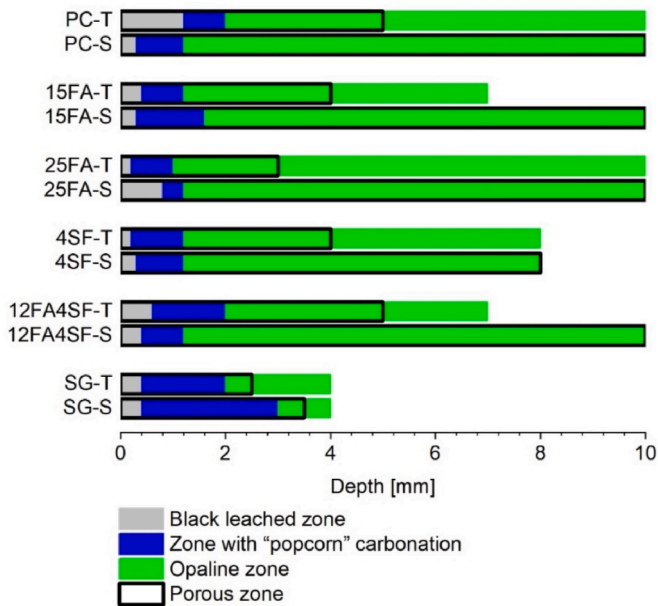
Fig. 6. Graphical representation of the extent of zonation observed by petrography on thin sections from the ten-year marine-exposed concretes. Note that the figure is simplified (in reality, the depth varies across the thin sections as seen in Fig. 5 for 4SF-T-W). Popcorn carbonation may be intermixed with the black leached zone. The opaline zone in SG was estimated from SEM-EDX data.

measuring 2–4 mm were placed in a glass test tube and sealed with a rubber plug. Duct tape was used to secure the rubber plug. The filled test tubes were placed in a temperature-controlled room ($22 \pm 2\,^\circ$C). The RH was measured with a Novasina HygroDat 100 system (sensor precision $\pm$ 0.5% RH in the range 11–95% at 25 $^\circ$C) and recorded daily starting from three days after placement in the analyzer.

A modified version [19] of the PF method originally proposed by Sellevold and Farstad [54] was used for porosity, DCS, and moisture content measurements. The method was applied both on concrete slices (labeled PF in Fig. 3) obtained by sawing (dry sample weight 63–120 g) and splitting (dry sample weight 413–569 g) – in both cases by using a scale with 0.01 g accuracy.

The capillary-saturated slices were dried at 50 $^\circ$C for six weeks with weekly measurements until a constant mass (<0.02% weight change/ day) was reached to obtain their dry weight after drying at 50 $^\circ$C (w_{dry50}), and then dried at 105 $^\circ$C for 17 days with a measurement after 16 days to conclude a constant mass (<0.02% weight change/day) was reached to obtain their dry weight (w_{dry105}).

The dry slices were again partly submerged in a water bath for one day to avoid trapping of air and thereafter fully submerged for four months, until a constant mass (<0.02% weight change/day) was reached, and then weighed in air (w_{sata-2}) and under water (w_{satw-2}) for control. Finally, the re-saturated slices were placed in a water-filled pressure tank exerting 5–15 MPa for two days and weighed within 2 min of releasing the pressure to prevent loss of water (w_{pres}).

The weights determined were used to calculate the following properties:

$$V = w_{sata} - w_{satw} \tag{3}$$

$$\text{Suction porosity at } 50^\circ\text{C ("capillary porosity")} = \left(w_{sata} - w_{dry50}\right) / V \tag{4}$$

$$\text{Macro porosity} = \left(w_{pres} - w_{sata}\right) / V \tag{6}$$

$$\text{Degree of capillary saturation} = \left(w_{start} - w_{dry105}\right) / \left(w_{sata} - w_{dry105}\right) \tag{7}$$

3. Results

3.1. Visual appearance and exposure

All concrete surfaces exhibited some organic growth. Fig. 4 shows a typical example of organic growth on a concrete panel right after pulling it out of the water. The part below mean tide level (red line, 1.3 m from the bottom) is covered with barnacles and mussels, the upper approx. 0.35 m is dry, and in between is a gradual transition from heavy to light organic growth.

All cores were taken in accordance with the coring plan (Fig. 2) from visually intact areas (without macroscopic cracks, scaling or mechanical damage). From Figs. 1 and 2, it can be deduced that the #8 cores from the tidal zone for petrography were submerged the vast majority of the time, while the #9 cores from the tidal zone for chloride analysis were submerged approximately half of the time with assumed frequent wetting from waves. Fig. 4 shows heavy organic growth with barnacles and mussels, not only on the submerged part of the panel, but also where the #9 cores for chloride analysis were taken.

3.2. Mechanical properties

Table 5 shows the compressive strength of cores extracted after ten years of exposure. The failure mode of all cores was normal, meaning compression failure at approx. the middle of the height of the core.

3.3. Microstructure

The petrographic analysis using optical polarizing microscopy showed that all the concretes exhibited a microstructurally changed zone in the outer approximately 10 mm of the panel after ten years of exposure. This zone comprised minor surface scaling, a leached and micro-cracked zone, a zone with bicarbonate precipitation, and a zone with a diffuse, opaline shine. The various microstructural features are explained in the following paragraphs, examples are shown in Fig. 5 and further details are found in Jakobsen et al. [10]. Table 6 and Fig. 6 summarize the depths to which the features were found.

All concretes exhibited uneven surfaces with exposed sand grains indicating minor surface scaling typically less than 0.5 mm in depth (Appendix D). Occasionally, the slightly scaled surfaces were covered by a thin calcite crust ($CaCO_3$), but without any sign of intermixing with brucite ($Mg(OH)_2$). The reason no brucite was observed might be that organic growth (as depicted in Fig. 4) has hampered the formation of a brucite layer for both exposure conditions [28].

From the surface to a maximum depth of 1 mm (Table 6), the paste appears completely black when viewed in cross-polarized light due to the depletion of calcium, not only from C–S–H but also from portlandite ($Ca(OH)_2$). This leached zone (Fig. 5, top left) contains brittle micro-cracks, many of which after ten years appear to have self-healed with calcium carbonate. Earlier SEM-EDX studies of the concrete showed that calcium in the former Ca-containing phases had been replaced by magnesium originating from sea water forming M-S-H. This is the main

$$\text{Suction porosity at } 105\ ^\circ\text{C ("capillary and gel porosity")} = \left(w_{sata} - w_{dry105}\right) / V \tag{5}$$
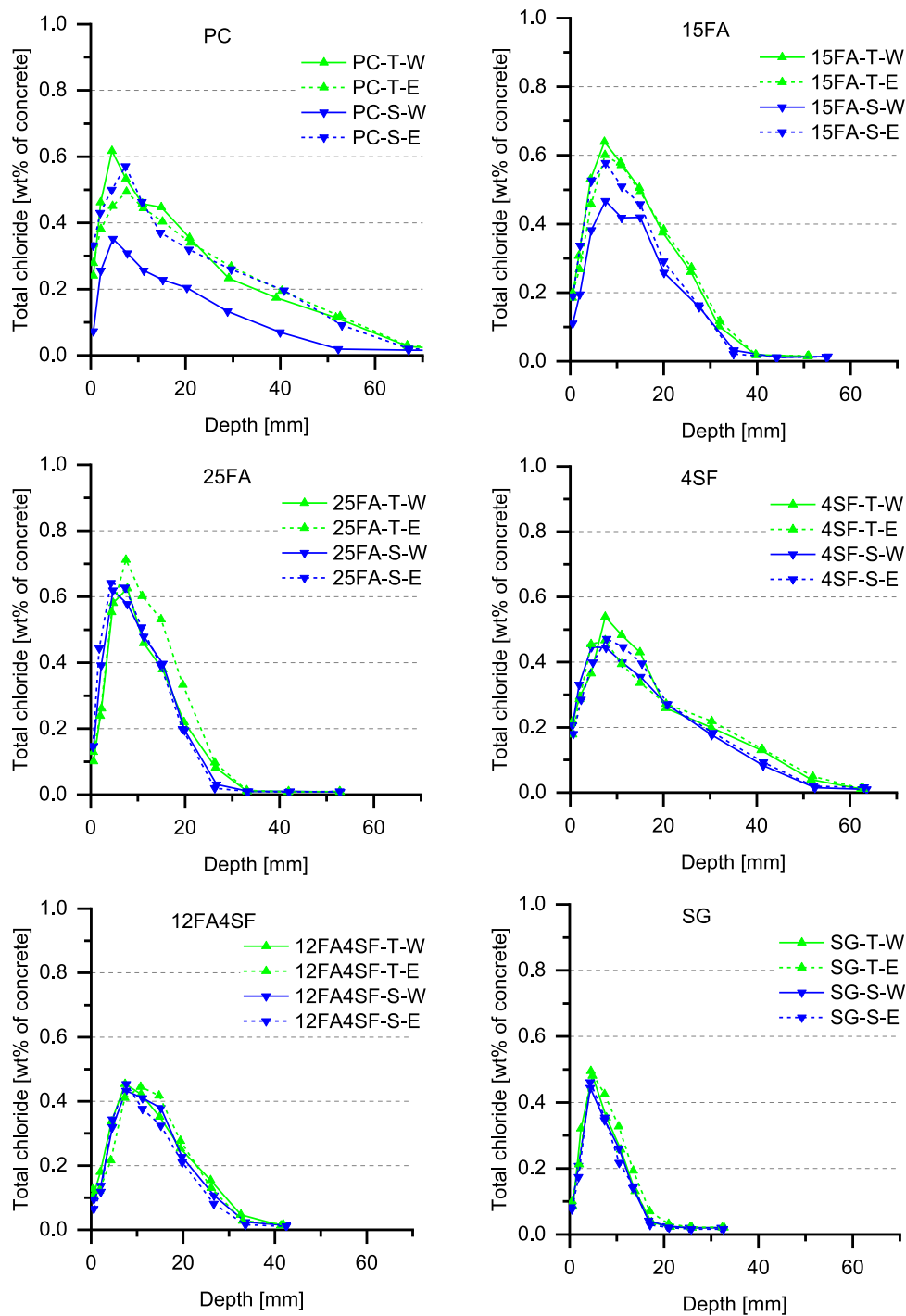
Fig. 7. Chloride profiles after 10 years of tidal (T) and submerged (S) exposure measured from the west and east-facing surfaces.

phase of the black zone.

Below and/or intermixed with the black leached zone, there is a zone containing a popcorn-like calcite formation to a maximum depth of 2 mm. The phrase "popcorn carbonation" describes the morphology. Popcorn carbonation is commonly observed when concrete is submerged in water rich in dissolved bicarbonate, resulting in a very distinct split of the paste into a decalcified C–S–H phase and a popcorn-like calcite phase (Fig. 5, top left). Typically, such a process results in a weakening of the paste [55,56].

The zone stretching deepest and about 10 mm into the concrete was optically observed to deviate from the bulk. In this zone, the paste appears somewhat micro-cracked and with a diffuse and opaline shine (Fig. 5 center). Earlier studies, including SEM-EDX analysis on the same concretes, have shown that this zone is enriched in both sulfur and chloride [10,13]. The special appearance of this so-called "opaline" zone is recognized in cross-polarized light in the optical polarizing microscope. The shine is due to infilling of the capillary pores, e.g., by secondary precipitation products such as ettringite. When the light in the polarizing microscope passes through such a "blocked" paste, it spreads in all directions making it difficult to identify individual phases in the paste such as portlandite.

In this study, the opaline zone was optically confirmed in all the
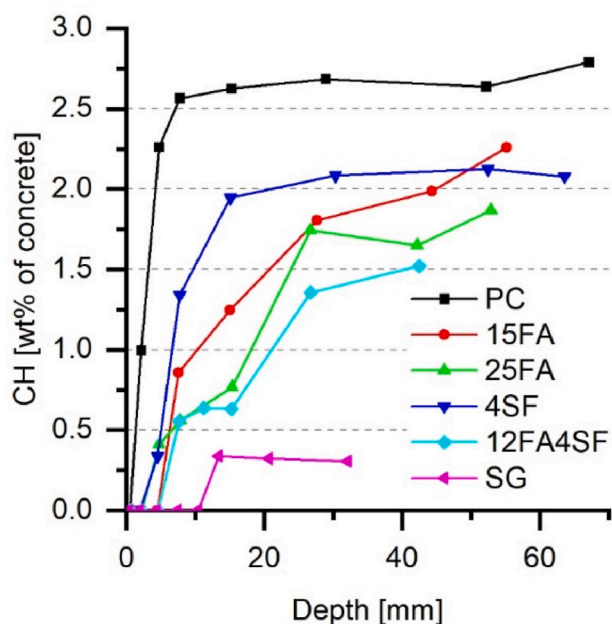
Fig. 8. Amount of portlandite (CH) as determined by TGA plotted against depth from the exposed surface for all the investigated concretes.

Table 7
Relative humidity [%] of a concrete piece taken from the center of a slice 40–70 mm from the east-facing surface of the #2 core from each of the six concretes and the temperature at which it was measured.

Concrete ID	PC	15FA	25FA	4SF	12FA4SF	SG
Relative humidity [%]	91	87	86	87	90	87
Temperature [°C]	22.3	22.3	22.3	22.2	22.2	22.3

concretes except the concrete containing slag (SG), as the highly dense texture of the slag concrete after 10 years exposure blurred the identification. In earlier studies using SEM-EDX, Jakobsen et al. [10] found that the depth of the opaline zone coincided with a sulfur enrichment of the paste, so in this study we also used SEM-EDX analysis to get a measurement for the depth of the opaline zone in the slag concrete (SG).

All the concretes showed higher porosity within the outer 10 mm of the concrete (Table 6). Using the fluorescent-light mode, the increased porosity observed in the surface region corresponds to an apparent *w/c* ratio of 0.70 or more (based on its green tone). The increased paste porosity stretched over the black leached and popcorn-carbonated zones as well as a part of the opaline zone (Table 6). Note the difference in green tone going from left to right in the bottom row in Fig. 5.

Table 6 gives the surface condition, maximum depth of zonation, micro-cracks (width <10 μm), and precipitation products for the tidal and submerged concrete in the investigated samples as the average depths to which they extend, and Fig. 6 shows the zonation in graphic form. All future references to depths of zonation in this paper refer to these depths. We observed that in all investigated panels the porous zone was deeper in the submerged exposed part than in the tidal exposed part. The opaline zone was generally similar for tidal and submerged exposure, except for concretes 15FA and 12FA4SF where the opaline zone was slightly deeper for submerged exposure. The depth of the opaline zone in SG was significantly less than for the remaining concretes in both tidal and submerged exposure.

3.4. Chloride content

Fig. 7 shows all the analyzed chloride profiles for ten years of

exposure organized by concrete. The same chloride profiles, but organized by exposure type, are shown in Appendix E. Appendix C shows the chloride profiles corrected for paste content using Eq. (1) in Section 2.2.5 and given as % by wt. of binder.

Out of all the chloride profiles determined after ten years of exposure, there seems to be one outlier, namely the PC-S-W, which shows considerably less chloride ingress than the other cores taken from the PC concrete (see Fig. 7, top left). The core from the neighboring position of the PC-S-W, which was extracted after two years, was also an outlier. This indicates a potential nonrepresentative concrete composition in this lower corner of the panel.

If using the penetration depth of 0.1% chloride by wt. of concrete as a measure for the chloride ingress resistance, the six concretes can after 10 years of exposure be ranked as follows for increasing chloride ingress resistance (independent of submerged or tidal exposure): PC < 4SF < 15FA < 12FA4SF < 25 FA < SG. It is noted that the shape of the chloride profiles for PC and 4SF is much flatter than for the remaining concretes.

3.5. Portlandite content

The portlandite content (CH) determined by TGA is shown in Fig. 8 as a function of depth from the exposed surface of all the analyzed concretes.

Four of the six investigated concretes show a near constant CH content in the deeper sections investigated. This CH content can be considered as the bulk CH content in the concrete. The highest bulk CH content is, as expected, observed for PC concrete. For the other concretes, the bulk CH content is lower due to the dilution of the Portland cement (which provides the CH) by the supplementary cementitious materials (SCMs) and due to the pozzolanic reaction of the SCMs (which consumes CH).

All CH profiles decrease towards the exposed surface, which can be mainly attributed to CH leaching in the outer zone [57]. However, enhanced reaction of the SCMs in this zone might also contribute to the decrease in the CH content. Nevertheless, calcium can still increase towards the surface due to the formation of a calcite crust and due to the wall effect during casting, which causes an increase in paste fraction towards the surface.

3.6. Moisture content and porosity

Table 7 gives the relative humidity of pieces taken from the center of a layer 40–70 mm from the east-facing surface of #2 cores. RH values in the range 86–91% were obtained, which are similar to those obtained by De Weerdt et al. [57], who reported RH values ranging between 88% and 92% at a depth of 70 mm in concrete submerged for 16 years. The values reported in Table 7 are single measurements. A similar setup was used by De Weerdt et al. [57], from which a standard deviation of approximately 1% RH was obtained on three replicates for a series of four concretes. Taking into account a similar standard deviation, there is no great difference between the concretes investigated in this study. There is, however, an indication that the PC concrete has a slightly higher RH than the SCM-containing concretes.

Fig. 9 shows the degree of capillary saturation (DCS) and porosity measured on the sawn slices and the split "bulk" samples from #2 cores. The depth of the data points shown in Fig. 9 represents the center of the slices used. The thickness of the slices varied between 8 and 15 mm as explained in Section 2.1.4. Thinner slices would have provided a more detailed graph, but the errors would increase due to the greater influence of water from sawing and the reduction in the sample size. The data points plotted at depth 115 mm correspond to 85 mm depth from the east-facing surface and relate to the measurements performed on the split "bulk" samples.

Fig. 9a and -b show the measured suction porosity as a function of depth from the west-facing surface relative to dry weight at 50 °C and 105 °C, respectively. The suction porosities are fairly similar for all six
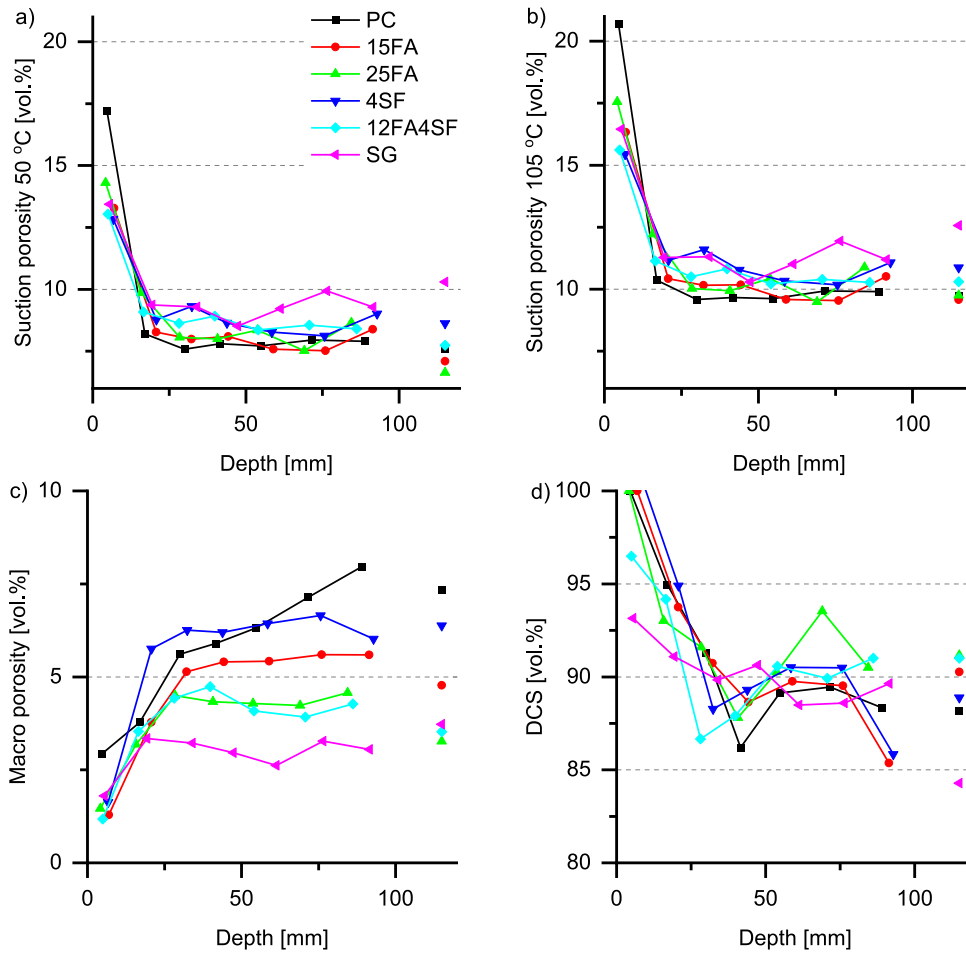
Fig. 9. Porosity and DCS of the sawn samples plotted at their average depth as well as split "bulk" samples taken at an average depth of 115 mm from the west-facing surface (85 mm from the east-facing surface): a) Suction porosity obtained by drying at 50 °C (capillary porosity); b) Suction porosity obtained by drying at 105 °C (gel and capillary porosity); c) Macro porosity; and d) DCS. Note that the outermost point is assumed to be too high due to insufficient cleaning of organic matter prior to measurement.
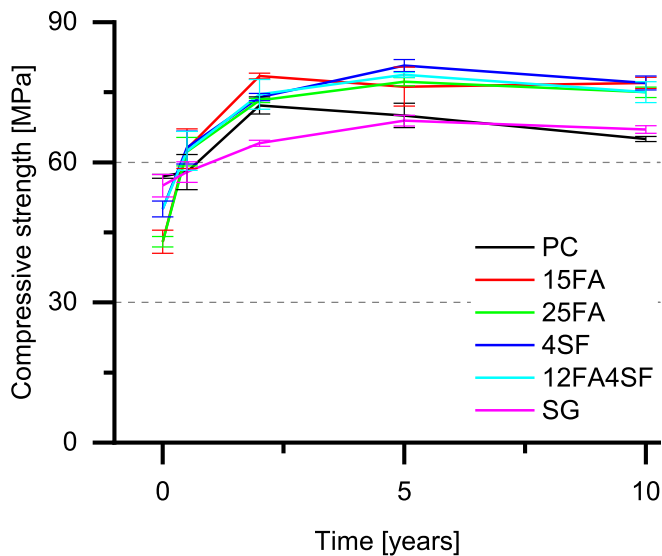
Fig. 10. Development in compressive strength with exposure time for all six concretes. Error bars show ± std. dev.

concretes. From a depth of approx. 15–130 mm, there are only minor variations, and they all seem to lie between 5 and 10% by vol. when expressed relative to the dry mass at 50 °C, and between 10 and 13% by vol. when expressed relative to the dry mass at 105 °C. All concretes showed an increase in the suction porosity of the outermost slice (approx. 8–13 mm) at the exposed surface, which can be expected due to the "wall-effect". As the exposed surface is a cast surface, the outermost zone cannot host large aggregate particles and consequently there was a higher paste content in these sections compared to the bulk. This higher paste content will give rise to a higher suction porosity. In addition, leaching might have led to an increase in the suction porosity due to the loss of material. From optical microscopy (see Fig. 6), the depth with higher porosity than the bulk, the porous zone, was measured to be approx. 10 mm for the submerged cores, which agrees well with the observed higher suction porosity in the outer 8–13 mm. The measured suction porosities agree well with De Weerdt et al. [19], who found suction porosities about 1% higher for concretes with slightly higher w/b ratios (0.42–0.44 vs. 0.4) and similar suction porosities for a concrete with w/b 0.4.

Fig. 9c shows the macro porosity of the concretes as a function of depth from the west-facing surface. The macro porosity seems to decrease in the outermost section. This could be due to either instability of air voids in the outermost section and/or filling of the air voids with reaction products, such as calcite, ettringite or thaumasite. The lower measured macro porosity in the outermost layer (ranging from 8 to 13 mm) agrees well with observations in the microscope, which showed
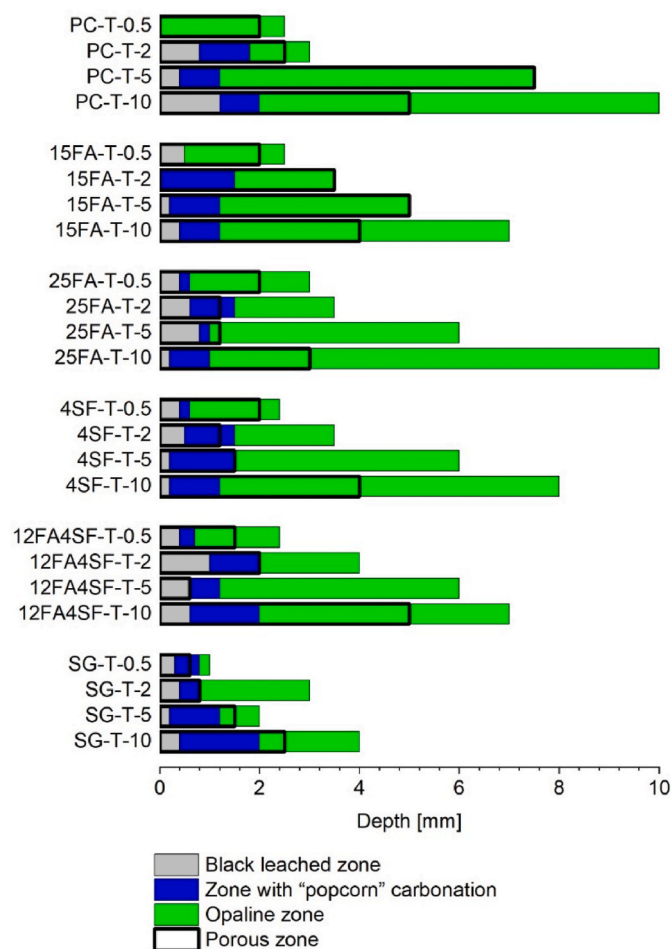
Fig. 11. Presence of zones (measured from the surface level at the time of coring) as observed after half a year, two, five, and ten years marine tidal exposure (west-facing panel sides). The opaline zone in SG was estimated from SEM-EDX data.

that excess ettringite was present in the air voids in the outer 6–13 mm (see Table 6). The measured macro porosity agrees well with the target air content of 3.5–5.5%, and that the air content was slightly above target for PC (5.8%), which shows the highest macro porosity in Fig. 9c. In comparison, De Weerdt et al. [19] found a macro porosity of approximately 1.8% independent of depth for concretes with a fresh air content of 3–3.6%.

Fig. 9d shows the DCS of the concretes as a function of depth from the west-facing surface. The reason the outermost point is above 100% for some concretes is assumed to be insufficient cleaning of organic matter prior to making the measurement. The consequence, according to the method described in 2.2.7, is a "w_{start}" that is too high, which causes the measured DCS to be too high in the outermost point. The measured porosities shown in Fig. 9a–c are expected to be unaffected. The DCS decreases from nearly saturated conditions at the surface to around 90% at a depth of approx. 30 mm and deeper in. The low bulk DCS shown in Fig. 9 and the RH values in Table 7 indicate self-desiccation, while the increase in DCS as the surface is approached indicates moisture uptake from the environment.

If we compare the results obtained on the sawn slices at a depth of for example 50–90 mm with the split bulk sample (depth 115 mm), they are in good agreement, indicating relatively little impact of water added from the water-cooled saw or from size-related uncertainties. The exception is the slag-containing concrete (SG), where DCS of the split bulk sample is around 5% less than for all the sawn samples of SG. We have no explanation for this single lower value, except that it might be a

measurement error.

4. Discussion

4.1. Material changes over time

4.1.1. Development of compressive strength

As binders hydrate, the porosity of concrete decreases and it becomes denser and gains strength [58]. As a check on the development of hydration at a macroscopic level, we determined the change in compressive strength over time. By comparing the measured compressive strength with previous results (Fig. 10, tabulated in Appendix F), we can see that the development of compressive strength stopped after five years. For most of our concretes, there was even a slight drop in the compressive strength over the following five years, but the reason for this slight drop is unknown.

There is not much in the literature on the long-term development (more than five years) in compressive strength. Generally, a slight increase in compressive strength is reported after five years [59–63], but a few papers show a decrease after five years of exposure for some concretes: OPC, SF and FA concretes with w/c 0.45–0.8 in hot and arid conditions in Kuwait [62], and SF concrete in field exposure, but not in laboratory-stored samples [61]. In a study of 50-year-old concretes exposed outdoors in northern USA, Washa and Wendt [59] found that the compressive strength of concretes made with coarsely ground cement with high C_2S content continued to increase over the 50-year period, whereas concrete made with finely ground cement and low C_2S content reached a maximum after 10–25 years. So, the above-mentioned literature suggests that a retrogression after five years in field-exposed concrete is uncommon, but not excluded.

For the concretes examined in this study, the outer 3 mm of each #3, #4 and #5 core end was ground off using a grinding cup to achieve a specimen flatness conforming with EN 12390-1 [47] prior to measuring the compressive strength. This means that the black leached zone with severe cracking as determined by optical polarizing microscopy in Section 3.3 was ground off, but not the entire depth with micro-cracks and chemical degradation, which reached deeper (see Table 6). The present data does not allow for further evaluation of the observed slight decrease in compressive strength after 10 years of exposure.

4.1.2. Development of zonation

For concrete exposed in the tidal zone, petrographic investigations, similar to those presented here for ten years exposed concrete, were carried out after half a year, two, and five years [44]. Fig. 11 shows a comparison of the observed development of zonation. Similar results were obtained from the west and east-facing sides of the panels, so only results from the west-facing surface of the panels are shown. We should note that, due to a lack of quantification of surface scaling (see Section 3.3 and Appendix D), a small offset of the depth has not been included in the figure.

There is no clear trend between exposure time and the depth for either the black leached zone or the popcorn-carbonated zone, which would be expected due to the ingress of magnesium and bicarbonate. This could be explained by the amount of surface scaling, which could be at significant levels when compared to the limited depths of these zones. A progressing surface scaling would effectively alter the starting point from which the depth is measured. The scaling after ten years of exposure is estimated to be around 0.5 mm, which is significant compared to the observed depth of both the black leached zone (0.2–1.2 mm) and the popcorn-carbonated zone (1–2 mm).

If we look at the depth of the opaline zone, which is much greater than the estimated scaling, there is a clear trend of increasing depth (and width) of the zone with increasing exposure time (Fig. 11).

Fig. 11 shows a trend of increasing depth of the porous zone with increasing exposure time. The depth of the porous zone is greater after ten years than after six months of exposure for all six concretes
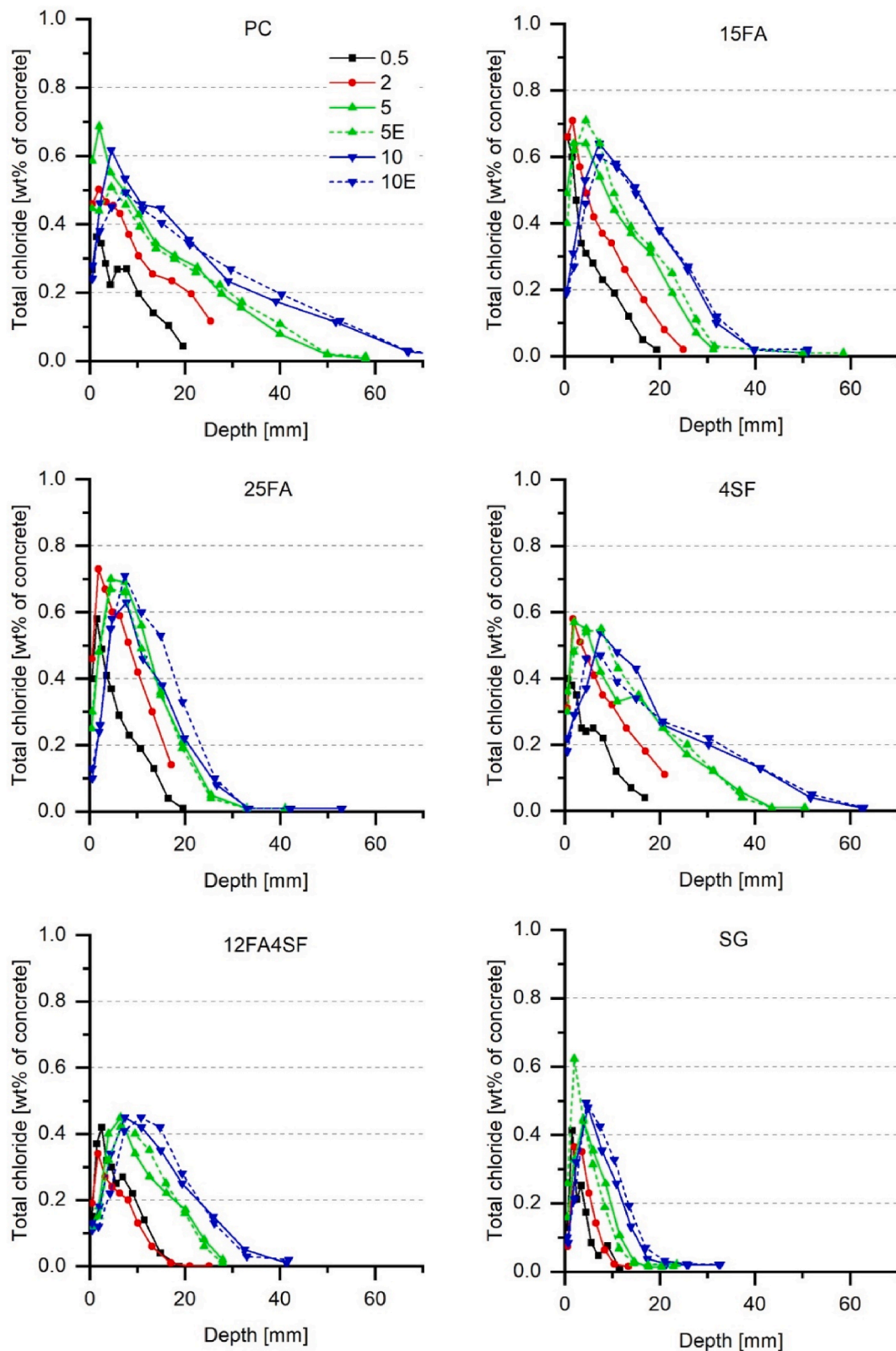
Fig. 12. Chloride profiles after half a year, two, five, and ten years in tidal exposure. All profiles are from the west-facing side of the panels, unless marked (E, dashed line) for the east-facing side.

(50–300% increase in depth depending on the concrete).

4.1.3. Development of chloride profiles

For comparison, chloride profiles from up to ten years of tidal and submerged exposure are plotted in Fig. 12 and Fig. 13, respectively.

With the exception of the outlier PC-S-W, all the chloride profiles measured after ten years show higher maximum chloride content (C_{max}) and deeper chloride penetration than for previous exposure times.
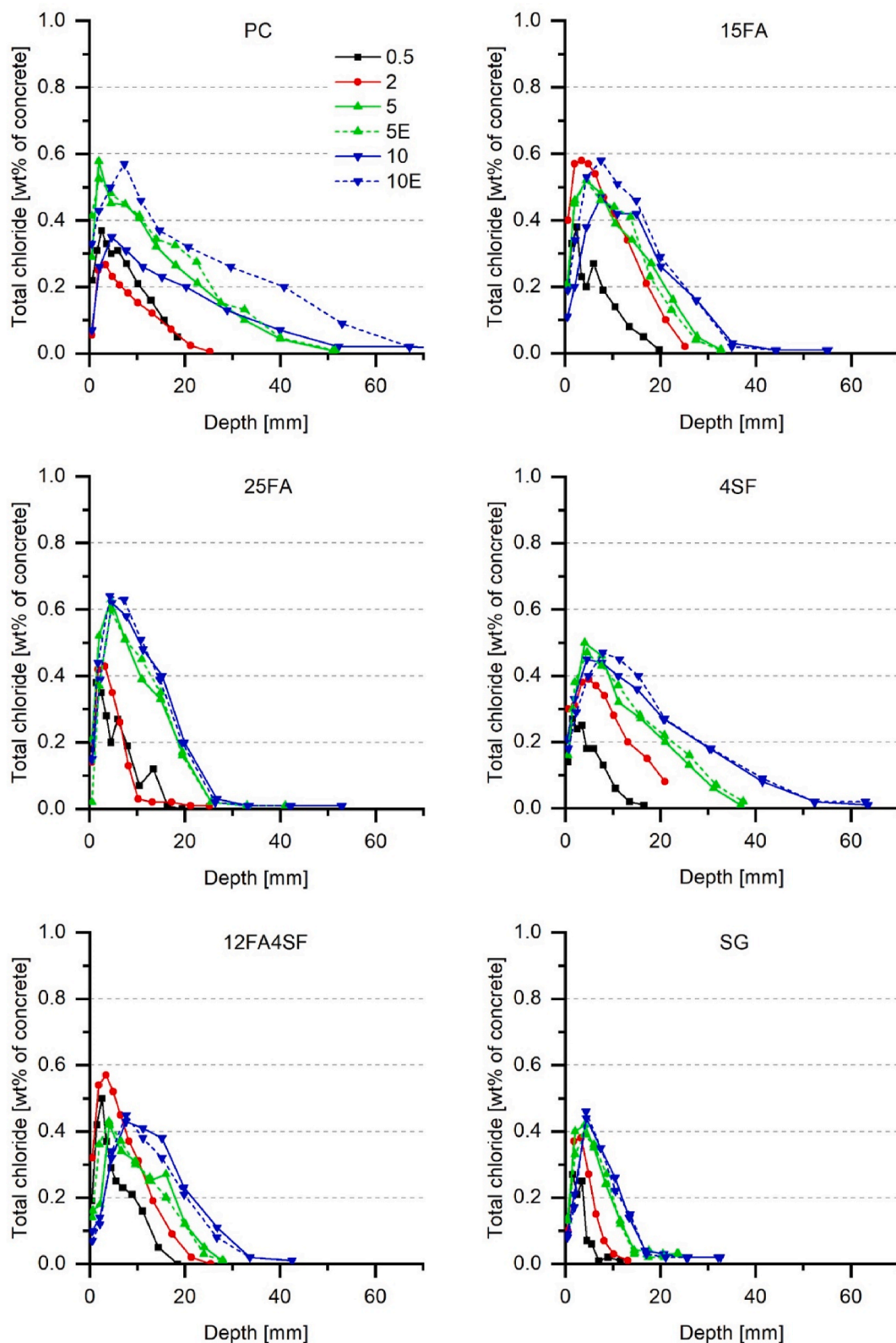
Fig. 13. Chloride profiles after half a year, two, five, and ten years in submerged exposure. All profiles are from the west-facing side of the panels, unless marked (E, dashed line) for the east-facing side.

Furthermore, when using the penetration depth of 0.1% chloride by wt. of concrete as a measure for the chloride ingress resistance, the ranking in chloride ingress resistance suggested for the blocks after five years by Poulsen et al. [1] is maintained after ten years of exposure (PC < 4SF <

15FA < 12FA4SF < 25 FA < SG). The increased resistance towards chloride ingress as a result of mineral additions and in particular GGBS is confirmed in numerous previous studies [64–66].

The progress of C_{max} and the position of the maximum chloride

Table 8

C_{max} [% by wt. of concrete] and the sampling interval that contains x_{Cmax} [mm] of chloride profiles obtained for tidal exposure for all measured exposure times and panel surfaces.

Exposure time [years] and orientation (W/E)	PC		15FA		25FA		4SF		12FA4SF		SG	
	C_{max} [% wt.]	x_{Cmax} [mm]	C_{max} [% wt.]	x_{Cmax} [mm]	C_{max} [% wt.]	x_{Cmax} [mm]	C_{max} [% wt.]	x_{Cmax} [mm]	C_{max} [% wt.]	x_{Cmax} [mm]	C_{max} [% wt.]	x_{Cmax} [mm]
0.6 W	0.36	1.4	0.66	0.6	0.58	1.6	0.38	1.5	0.42	2.5	0.41	1.5
2 W	0.50	1.9	0.71	1.7	0.73	1.8	0.58	1.7			0.37	2.1
5 W	0.69	1.9	0.64	4.5	0.70	4.5	0.57	2.0	0.43	4.0	0.44	3.9
5 E	0.51	4.5	0.71	4.5	0.67	4.4	0.55	7.7	0.42	6.5	0.62	2.0
10 W	0.62	4.5	0.64	7.3	0.63	7.7	0.54	7.5	0.45	7.4	0.48	4.9
10 E	0.49	7.6	0.60	7.4	0.71	7.4	0.47	7.5	0.45	11	0.50	4.5

content (x_{Cmax}) obtained from the chloride profiles for tidal exposure shown in Fig. 12 are tabulated in Table 8. We should note that the tabulated x_{Cmax} is the middle of the section in which it is present. The thickness of the sections varied with the depth from surface, the exposure time, and the binder (approx. 1 mm for the outermost section, 2 mm for the second, 3 mm for the following two, and 4 mm for the fifth section – the deepest section containing any C_{max} in this study). In contrast to the actual maximum chloride content and its position in a sample, the measured C_{max} and x_{Cmax} depends on the thickness of the respective section. For the measured C_{max}, the chloride content is averaged over the section, thus a thicker section might result in a lower C_{max}. This could for example be the reason why the measured C_{max} is higher for 15FA, 25FA and SF after two years than after ten years: the values after two years were averaged over a sample spanning 1 mm, compared to the values after ten years which were the average of a 3 mm depth increment.

Table 8 shows that the position of the highest chloride content, x_{Cmax}, gradually moves towards greater depths with time. The shift of x_{Cmax} towards greater depths is related to phase changes. This topic is further discussed in 4.3. After ten years of exposure, x_{Cmax} is reached at a depth of 4–11 mm from the surface, depending on binder type. The lowest penetration depth is seen for SG.

Based on the C_{max} values given in Table 8, initially C_{max} increases, but already after two years, it appears stable. There was a slight decrease in the C_{max} values for some concretes after ten years compared to the C_{max} values after two years, e.g., for 15FA and 25FA. This is due to the difference in section thickness where the C_{max} occurs, as mentioned earlier. After two years the C_{max} value is averaged over a 1 mm interval, whereas the C_{max} value after ten years is the average of a 3 mm depth increment.

Table 8 also shows that C_{max} as a general trend is higher for the concretes containing fly ash as the only SCM than for the remaining concretes. This agrees with Taylor's statements Taylor [30] that "*With Portland cements, the Cl⁻/OH⁻ ratios decreased with potential C₃A content; cements containing 30% FA or 65% GGBS gave lower ratios than any of the Portland cements. The OH⁻ concentrations were lower for the composite cements, and the low Cl⁻/OH⁻ were presumable due to greater uptake of Cl⁻ in the hydration products*" and "*replacement of cement by silica fume may be expected both to lower the OH⁻ concentration and to decrease the content of AFm phase able to take up Cl⁻*".

The combination of a relatively high C_{max} for fly ash concretes and a good chloride ingress resistance resulted in steep chloride profiles for 15FA and 25FA. In contrast, for 4SF a lower binding capacity and a poorer chloride ingress resistance resulted in a flatter chloride profile. This tendency was observed to become more pronounced with time.

4.2. Tidal vs. submerged

In the panels we investigated no major differences were observed in the microstructural changes and chloride profiles between concrete exposed to tidal and submerged conditions for ten years. The extent of zonation, micro-cracks, and precipitated products in voids were

comparable, but the surface was typically less scaled for submerged exposure (see Table 6 and Fig. 6), which is for instance in agreement with Mehta [15], and the chloride profiles showed only slightly higher peaks for tidal exposure, where also slightly deeper ingress was observed (Fig. 7).

One explanation for the similar observations could be that the actual exposure conditions were to a large extent similar. Figs. 1 and 2 indicate that the #9 cores for chloride analysis from the tidal zone were submerged approximately half of the time, with assumed frequent wetting from waves. Moreover, Fig. 4 shows heavy organic growth with barnacles and mussels not only on the submerged part of the blocks, but also in the tidal zone where the #9 cores for chloride analysis were taken. Both frequent wetting and organic growth prevent drying and accumulation of chloride at the evaporation front, which could explain why the maximum chloride content is only slightly higher for the chloride profiles obtained from tidal exposure than for those from the submerged exposure.

4.3. Correlation of chloride profiles with microstructural and moisture changes for submerged exposure

Fig. 14 shows a comparison of the depth of the microstructurally changed zone (x_{MCZ}), and the chloride, DCS and CH profiles for all six concretes after ten years of submerged exposure. The influence of moisture, microstructural changes as observed in optical polarizing microscope, and measured CH profiles on chloride ingress is discussed in subsections 4.3.1, 4.3.2 and 4.3.3 respectively.

4.3.1. Effect of moisture content on chloride ingress

The chlorides present as free chlorides in the suction porosity only represent a fraction of the total chloride content. If we consider a suction porosity of 10% by volume or 100 L/m³ concrete, which is a fair assumption when we look at Fig. 9, and fill this hypothetically with sea water (7 g Cl/L, see Table 2), this would create a chloride content of 0.7 kg/m³ concrete. If we divide this by the density of the concrete, 2383 kg/m³ (PC concrete in Table 1), we obtain a chloride content of 0.03% by wt. of concrete, which is similar to the background level. This suggests that a major part of the chlorides we measure are not free but bound [24].

Nevertheless, porosity and the DCS play a major role when it comes to the ingress of chlorides. This is illustrated in Fig. 14, where the chloride profiles are compared to the change in DCS measured with depth. The chloride concentration decreases to the background level shortly after the DCS reaches the bulk level. This is explained by a reduced diffusion rate of chlorides when the DCS decreases, as found by Nielsen and Geiker [6] and Olsson et al. [7]. At a DCS of 85–89% as found in this study, the effective diffusion coefficient was found by Olsson et al. [7] to decrease to approximately 45–75% compared to saturated conditions.

4.3.2. Relationship between microstructural changes and chloride profiles

In Fig. 14, the depth of the maximum chloride content (x_{Cmax}) for all
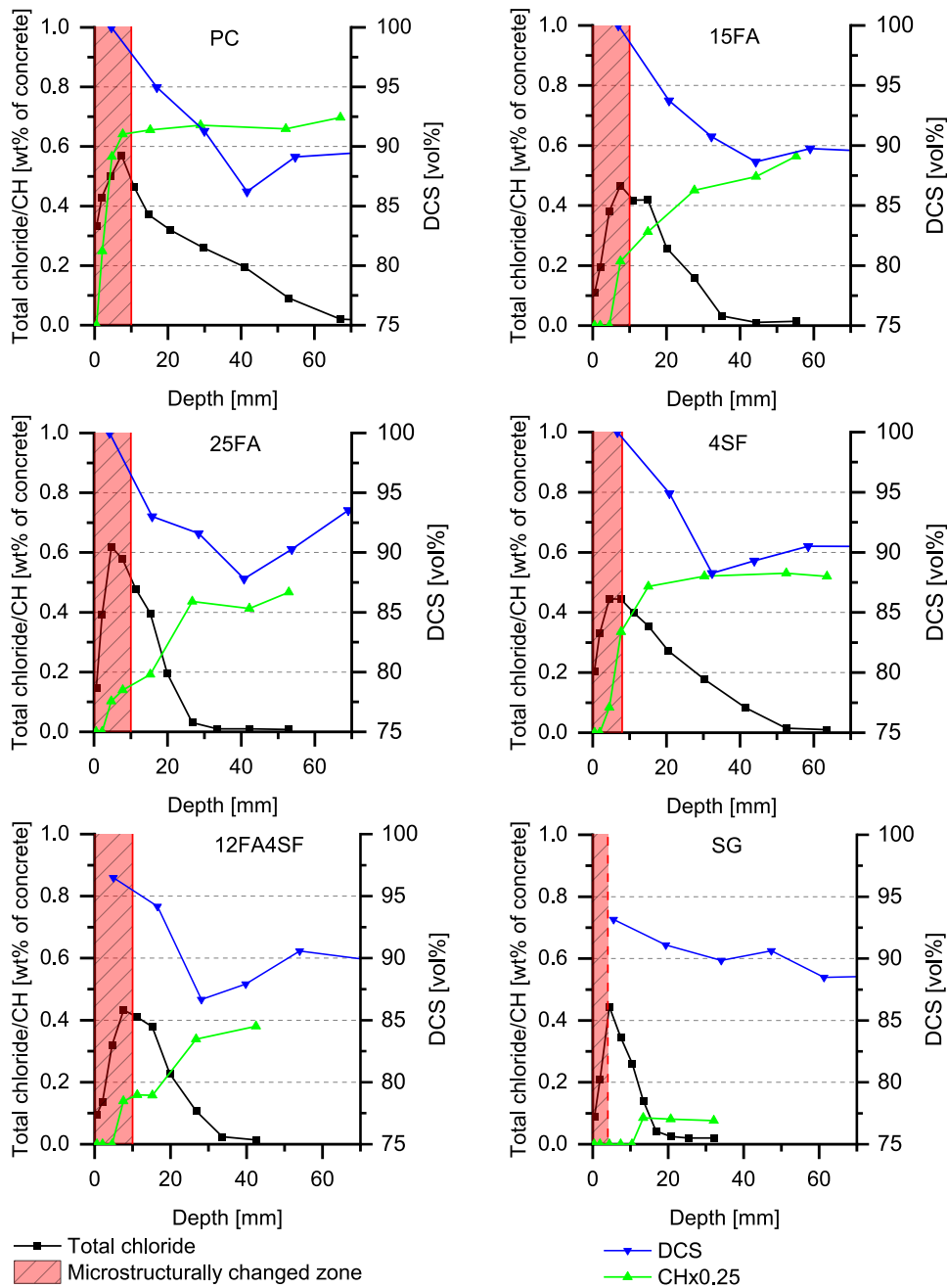
Fig. 14. Depth of observed microstructurally changed zone compared to corresponding chloride, DCS and portlandite (CH) profiles after ten years of submerged exposure. To fit the results in one graph, CH has been scaled to one fourth. The chloride profile and CH are given as % by wt. of concrete, whereas the DCS is in % by vol. The titles correspond to the concrete compositions. Note that for PC the chloride profile shown is from the east-facing surface. The microstructurally changed zone in SG was estimated from SEM-EDX data (dashed red line). (For interpretation of the references to colour in this figure legend, the reader is referred to the Web version of this article.)

concretes coincides with the inner part of the microstructurally changed zone. This observation is in line with previous observations on concretes exposed to sea water [19,27], including those analyzed in this paper but at earlier exposure times [10]. Jakobsen et al. [10] and De Weerdt et al. [19] found that C_{max} followed immediately after the sulfur-enriched zone. They explained that the low chloride content in the outermost black leached zone might be due to a low chloride binding capacity of M-S-H [10,57] and the decomposition of chloride-containing AFms in the low pH of this zone. In the sulfur-rich microstructurally changed zone, the chloride binding in the paste decreases due to the preferred binding of sulfates with aluminates in AFts and the adsorption of sulfates in C–S–H [20,27]. As a result, the maximum chloride content in the

paste is observed at the deeper end of the sulfur-rich zone.

Fig. 15 shows the relationship between x_{MCZ} (shown as the abscissa) and the x_{Cmax}, (shown as the ordinate). Data for the tidal zone can cover half a year or two, five or ten years, whereas only ten-year data are available for the submerged zone. The diagonal dotted line, x = y, is included as a guide for the eye. Note that some scatter is to be expected because x_{Cmax} is the mean value of a depth interval varying in thickness between 1 and 3 mm, while x_{MCZ} is determined on a thin section taken perpendicular to the surface, but only representing 40 mm × 20 μm at each depth. This is important with regard to both the accuracy and the representative sample volume. For the tidal exposed concrete, x_{Cmax} and x_{MCZ} appear to coincide, whereas the few data from the submerged zone
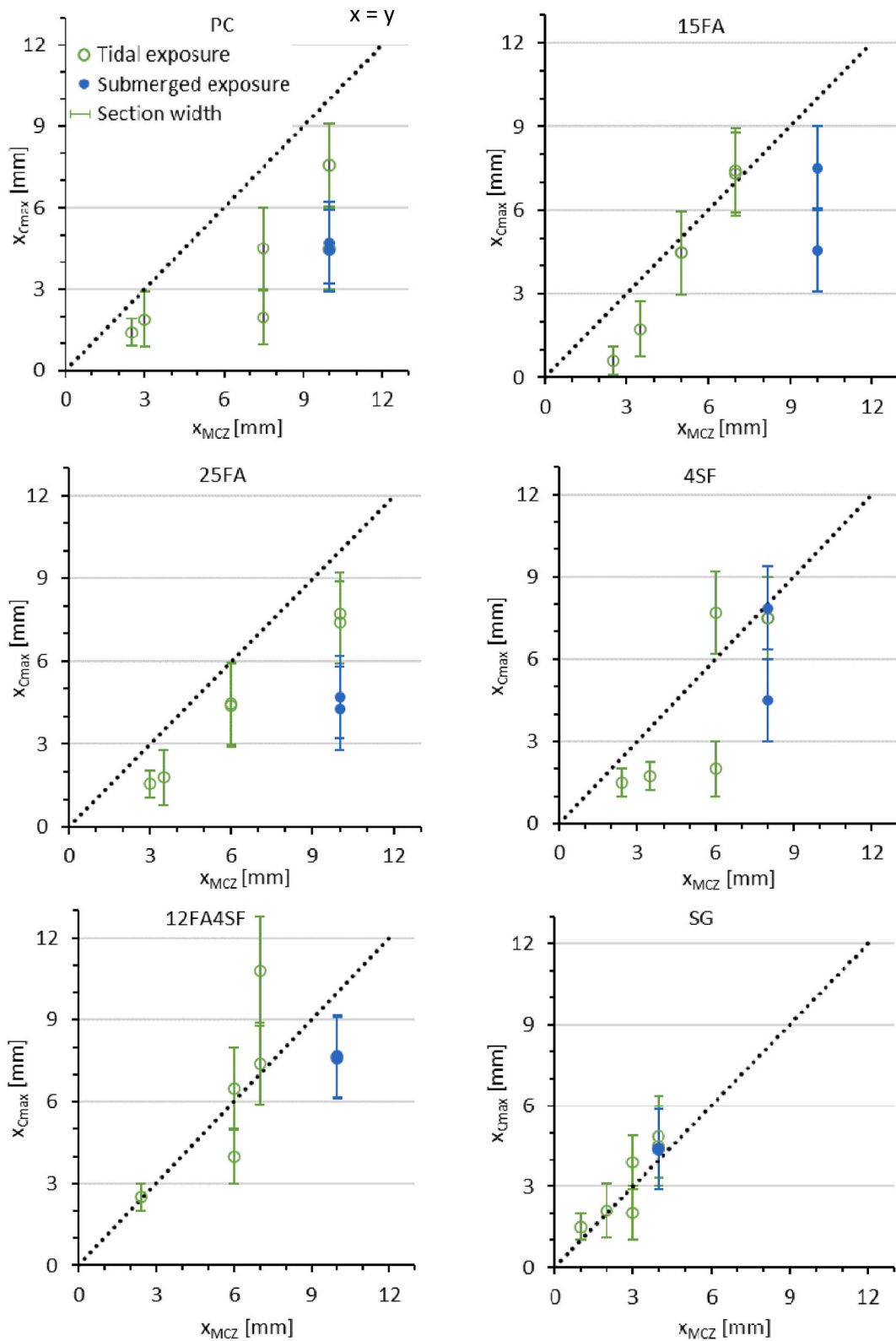
Fig. 15. Comparison of the depth of the microstructurally changed zone (x_{MCZ}) with the depth of maximum chloride content (x_{Cmax}). x_{Cmax} from both the west and east-facing surfaces of the panels are included to give an impression of the uncertainties. Unfilled circles = tidal exposure (for half a year or two, five or ten years). Filled circles = submerged exposure (for ten years). The lines (error bars) indicate the width of sections. x = y is indicated with a dotted line as a guide for the eye.

indicate that in this zone x_{Cmax} precedes x_{MCZ}. This is to be expected because x_{Cmax} should coincide with the deeper end of the microstructurally changed zone, i.e., the end of the sulfur-enriched zone, as mentioned above.

To elucidate the relationship between x_{MCZ} and x_{Cmax} as a function of time, x_{Cmax}, is compared with x_{MCZ} as a function of exposure time for all six concretes in Fig. 16 and Appendix G. Both x_{MCZ} and x_{Cmax} gradually move inwards over time, and the microstructurally changed zone, x_{MCZ},
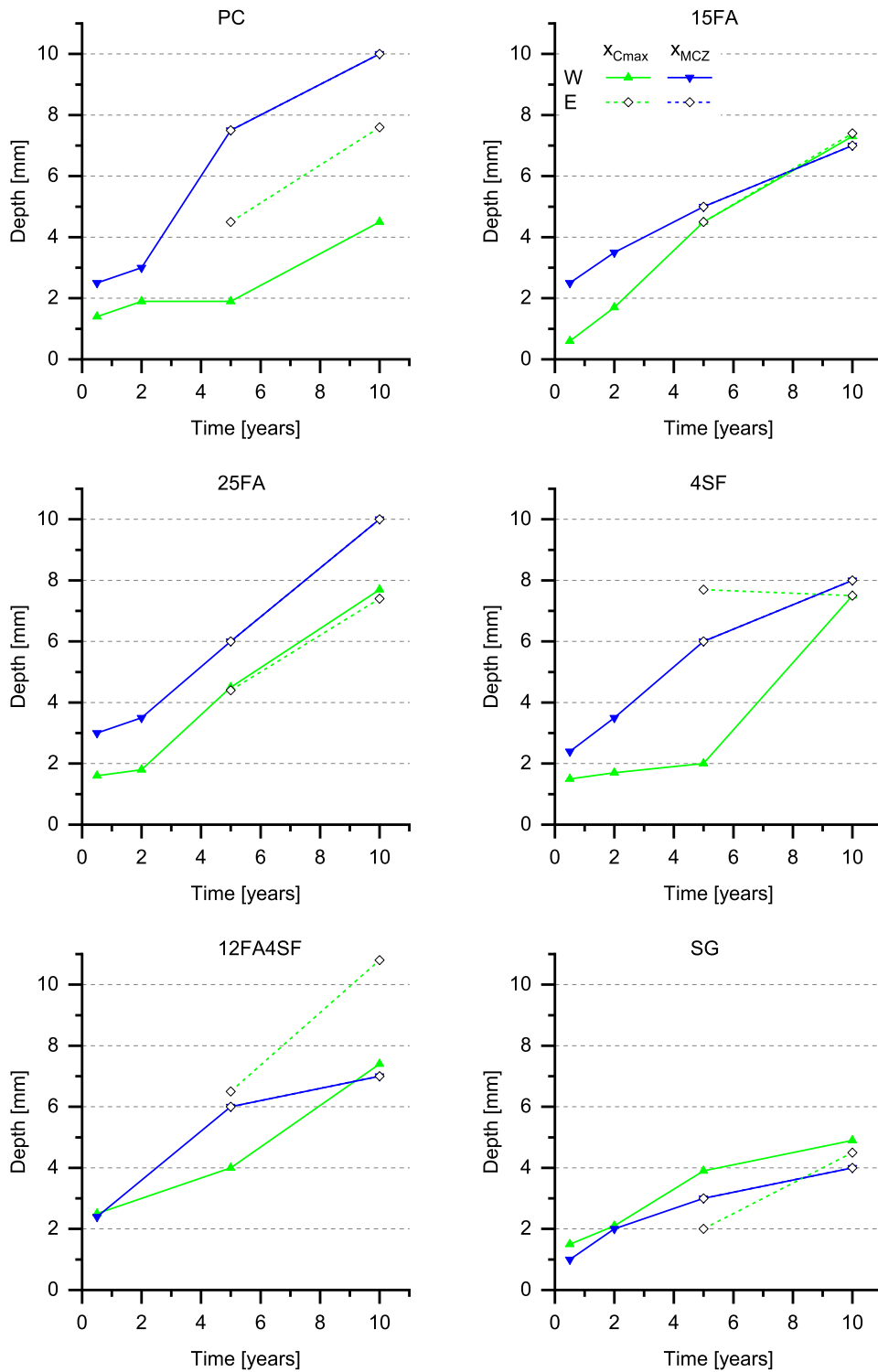
Fig. 16. Development of chloride peak depth (x_{Cmax}) and the depth of microstructurally changed zone (x_{MCZ}).

reaches a depth of 4–10 mm after ten years in the concretes investigated. This zone will have altered diffusion characteristics, which should be taken into account, when predicting chloride ingress. This topic is dealt with in Section 4.4.

4.3.3. Relationship between the portlandite profiles and chloride ingress profiles

Fig. 14 also enables us to study the relationship between the portlandite (CH) profiles and the chloride ingress and DCS profiles, as well

as the depth of the microstructurally changed zone for the investigated concretes. The decrease in the CH profiles towards the exposed surface gives an indication of the extent of leaching, because CH is one of the first hydrates to dissolve upon leaching [67]. In the case of the PC, SF, and SG concretes, the leaching depth (as indicated by a clear drop in the CH content) seems to agree rather well with the depth of the microstructurally changed zone. In the case of the concretes containing fly ash (15FA, 25FA and 12FA4SF), the gradual decrease in CH continues beyond the microstructurally changed zone and tends to level out only at

greater depths. This could be due to the pozzolanic reaction of the fly ash in the zone behind the microstructurally changed zone. In this zone, the pH could still be sufficiently high to activate the pozzolanic reaction and the DCS has not fallen to the background level, which indicates that there is moisture available for the reaction. A gradual decrease in CH that only levels out at greater depths was also found by De Weerdt et al. [57], who suggested it might be due to pozzolanic reaction. Furthermore, Frías et al. [68] found that the CH content decreases more in pastes containing fly ash than in PC paste, when immersed in aggressive solutions containing chloride and/or sulfate. This potential pozzolanic reaction and consequent continuous refinement of the pores in the concretes containing fly ash might, in combination with increased binding [69], explain the sharper decrease in the chloride content in this zone for the concretes containing fly ash than for the others [70]. Note that the decrease in portlandite could not be explained by carbonation, as the depth of carbonation was 1–3 mm, whereas the depth of leaching was 10–15 mm. Comparable depths of carbonation were found in tidal and submerged exposure.

4.4. Recommendations on valid depth for verification of chloride ingress prediction models

In this study, a microstructurally changed zone was observed to occur both in the tidal and the submerged zones of marine-exposed concretes (Section 4.3). The depth of microstructural changes (x_{MCZ}) increased over time and correlated with the depth of the maximum chloride content (x_{Cmax}).

Based on the observed relationship between the evolution of x_{MCZ} and x_{Cmax}, it is recommended that only chloride data from sections taken deeper than the microstructurally changed zone are used from field data when assessing the remaining service life of structures and when verifying chloride ingress prediction models, unless reactive transport models are used. For the data presented here for six concrete panels exposed for ten years, this exclusion includes the chloride peak.

The observed gradual progression of x_{MCZ} and x_{Cmax} means that the approach proposed by Andrade et al. [40] for assessment of cases where neither the C_{max} nor x_{Cmax} are time-dependent is not applicable.

The square root method is an example of a reassessment method that can be applied in cases where a gradual development of C_{max} and/or x_{Cmax} occurs. The method excludes the microstructurally changed zone by omitting the data point corresponding to C_{max} and all data points closer to the surface [3]. However, the application of the method for design purposes requires available model parameters for the concrete and exposure in question, which necessitates either the use of well-known concretes or a relatively long period of pretesting [3].

For design purposes, reactive transport models, e.g. Stadium [71], DuCOM [72], etc., provide the possibility of predicting the entire chloride profile including the interaction between multiple species. However, to the best of the author's knowledge, their general usage is limited, perhaps due to their complexity and because not all information is disclosed.

5. Conclusion

Based on ten years of field data for 0.4 *w/c* concrete panels differing in binder composition (plain CEM I and blends with fly ash and/or silica fume, and slag) from the Fehmarn Belt Exposure Site combined with earlier data obtained after a half-year, two, and five years of submerged and tidal exposure, we conclude that:

- After ten years of exposure, chloride profiles from the submerged and the tidal zones were to a large extent comparable. A peaking behavior was observed, and the depth of the maximum chloride content (x_{Cmax}) progressed inwards over time in panels subjected to both tidal and submerged exposure. In general, the maximum chloride content was less than 10% higher for the tidal exposure than for

the submerged exposure. Deepest ingress was found in the concretes with plain CEM I and CEM I mixed with 4% silica fume.

- A microstructurally changed zone was a generally observed feature in the outer approximately 10 mm of all six concretes after ten years of exposure, independent of the binder composition and exposure. Starting from the exposed surface, we observed: minor surface scaling, a black leached and microcracked zone rich in magnesium, a zone with bicarbonate precipitation, and a zone with a diffuse opaline shine, rich in sulfur. Comparison with earlier data showed that the depth of the microstructurally changed zone progressed inwards over time.

- A correlation was observed between chloride profiles and microstructural changes. The depth of the maximum chloride content (x_{Cmax}) was found to almost coincide with the depth of the microstructurally changed zone (x_{MCZ}). A binder-dependent increase was observed in x_{Cmax} from 0.6 to 2.5 mm after six months to 4.5–10 mm after ten years, and in x_{MCZ} from 1 to 2.5 mm after six months to 4–10 mm after ten years; the least increase was observed for concrete containing slag.

- Limited moisture ingress combined with self-desiccation caused the degree of capillary saturation to increase towards the exposed surface from a bulk level of about 90% at a depth of 30–40 mm of the submerged concrete. This lower DCS in the bulk will limit further chloride ingress by diffusion. Due to leaching in the outer zone, all portlandite profiles decreased from a bulk level towards the exposed surface. For the concretes containing fly ash, moisture ingress and portlandite depletion progressed to a depth far beyond that of the microstructurally changed zone.

Based on the above conclusions, we recommend that data from the microstructurally changed zone should be excluded when using field data for verification of chloride ingress prediction models, unless reactive transport models are used. Because the depth of the microstructurally changed zone coincides with the depth of the maximum chloride content, for practical purposes, we recommend only using data from greater depths.

Declaration of competing interest

The authors declare that they have no known competing financial interests or personal relationships that could have appeared to influence the work reported in this paper.

Appendix A. Supplementary data

Supplementary data to this article can be found online at https://doi.org/10.1016/j.cemconcomp.2022.104590.

References

[1] S.L. Poulsen, H.E. Sørensen, U. Jönsson, Chloride ingress in concrete blocks at the Rødbyhavn marine exposure site – status after 5 years, in: 4th International Conference on Service Life Design for Infrastructures (SLD4), Delft, Netherlands, 2018, pp. 192–203.

[2] U.H. Jakobsen, Petrografic Evaluation after 5 Years of Exposure to Seawater, 2015. http://www.expertcentre.dk/media/25643/petrographic_evaluation_5_years.pdf. (Accessed 22 February 2021).

[3] S. Fjendbo, H.E. Sørensen, K. De Weerdt, M.R. Geiker, The square root method for chloride ingress prediction—applicability and limitations, Mater. Struct. 54 (2021), https://doi.org/10.1617/s11527-021-01643-8, 61.

[4] M.R. Geiker, H. Justnes, Prediction of Chloride Induced Corrosion for Service Life Modelling, 1st International Congress on Durability of Concrete, Trondheim, Norway, 2012.

[5] A.V. Saetta, R.V. Scotta, R.V. Vitaliani, Analysis of chloride diffusion into partially saturated concrete, Materials Journal 90 (5) (1993) 441–451.

[6] E.P. Nielsen, M.R. Geiker, Chloride diffusion in partially saturated cementitious material, Cement Concr. Res. 33 (1) (2003) 133–138, https://doi.org/10.1016/S0008-8846(02)00939-0.

[7] N. Olsson, B. Lothenbach, V. Baroghel-Bouny, L.-O. Nilsson, Unsaturated ion diffusion in cementitious materials–The effect of slag and silica fume, Cement Concr. Res. 108 (2018) 31–37, https://doi.org/10.1016/j.cemconres.2018.03.007.

[8] N. Olsson, F.A. Wahid, L.-O. Nilsson, C. Thiel, H.S. Wong, V. Baroghel-Bouny, Wick action in mature mortars with binary cements containing slag and silica fume–The relation between chloride and moisture transport properties under non-saturated conditions, Cement Concr. Res. 111 (2018) 94–103, https://doi.org/10.1016/j.cemconres.2018.06.006.

[9] M.A. Climent, G. De Vera, J.F. López, C. García, C. Andrade, J. Kropp, Transport of chlorides through non-saturated concrete after an initial limited chloride supply, in: C. Andrade, K. J (Eds.), Second International RILEM Workshop on Testing and Modelling the Chloride Ingress into Concrete, RILEM Publications SARL, 2000, pp. 173–187.

[10] U.H. Jakobsen, K. De Weerdt, M.R. Geiker, Elemental zonation in marine concrete, Cement Concr. Res. 85 (2016) 12–27, https://doi.org/10.1016/j.cemconres.2016.02.006.

[11] J. Marchand, E. Samson, D. Burke, P. Tourney, N. Thaulow, S. Sahu, Predicting the Microstructural Degradation of Concrete in Marine Environment, vol. 212, Special Publication, 2003, pp. 1127–1154.

[12] A. Chabrelie, E. Gallucci, K. Scrivener, U. Müller, Durability of Field Concretes Made of Portland and Silica Fume Cements under Sea Water Exposure for 25 Years, Nordic Exposure Sites – Input to Revision of EN206-1, Hirtshals, Denmark, 2008, pp. 275–294.

[13] U.H. Jakobsen, Microstructural Surface Deterioration of Concrete Exposed to Seawater; Results after 2 Years of Exposure, 14th Euroseminar on Microscopy Applied to Building Materials, Helsingør, Denmark, 2013.

[14] P.K. Mehta, P.J. Monteiro, Concrete: Microstructure, Properties, and Materials, McGraw-Hill Education, 2014.

[15] P.K. Mehta, Durability of concrete in marine environment – a review, in: V. M. Malhotra (Ed.), Performance of Concrete in Marine Environment, 1980, pp. 1–20. ACI SP-65.

[16] Y.-J. Tang, X.-B. Zuo, G.-J. Yin, H. Davoudi, X.-N. Li, Influence of calcium leaching on chloride diffusivity in cement-based materials, Construct. Build. Mater. 174 (2018) 310–319, https://doi.org/10.1016/j.conbuildmat.2018.04.112.

[17] F.P. Glasser, J. Marchand, E. Samson, Durability of concrete – degradation phenomena involving detrimental chemical reactions, Cement Concr. Res. 38 (2) (2008) 226–246, https://doi.org/10.1016/j.cemconres.2007.09.015.

[18] P. Hemstad, A. Machner, K. De Weerdt, The effect of artificial leaching with HCl on chloride binding in ordinary Portland cement paste, Cement Concr. Res. 130 (2020), 105976, https://doi.org/10.1016/j.cemconres.2020.105976.

[19] K. De Weerdt, D. Orsáková, A.C.A. Müller, C.K. Larsen, B.M. Pedersen, M.R. Geiker, Towards the understanding of chloride profiles in marine exposed concrete, impact of leaching and moisture content, Construct. Build. Mater. 120 (2016) 418–431, https://doi.org/10.1016/j.conbuildmat.2016.05.069.

[20] K. De Weerdt, D. Orsáková, M.R. Geiker, The impact of sulphate and magnesium on chloride binding in Portland cement paste, Cement Concr. Res. 65 (2014) 30–40, https://doi.org/10.1016/j.cemconres.2014.07.007.

[21] K. De Weerdt, H. Justnes, The effect of sea water on the phase assemblage of hydrated cement paste, Cement Concr. Compos. 55 (2015) 215–222, https://doi.org/10.1016/j.cemconcomp.2014.09.006.

[22] M. Geiker, Fly Ash in Concrete, Danish Experience, Norwegian Public Roads Administration, 2015.

[23] B.B. Jensen, R. Sørensen, T. Frølund, M. Sloth, T. Johnsen, E. Stoltzner, Farøbroerne. Betonundersøgelser 1988-2005, COWI, 2006.

[24] K. De Weerdt, Chloride Binding in Concrete – Recent Investigations and Recognised Knowledge Gaps: RILEM Robert L'Hermite Medal Paper 2021, Materials and Structures in press.

[25] A. Machner, M.H. Bjørndal, H. Justnes, L. Hanžič, A. Šajna, Y. Gu, B. Bary, M. Ben Haha, M.R. Geiker, K. De Weerdt, Effect of leaching on the composition of hydration phases during chloride exposure of mortar, Cement Concr. Res. 153 (2022), 106691, https://doi.org/10.1016/j.cemconres.2021.106691.

[26] W. Kunther, B. Lothenbach, K.L. Scrivener, On the relevance of volume increase for the length changes of mortar bars in sulfate solutions, Cement Concr. Res. 46 (2013) 23–29, https://doi.org/10.1016/j.cemconres.2013.01.002.

[27] P.K. Mehta, Concrete in the Marine Environment, first ed., CRC Press, London, 2019.

[28] N.R. Buenfeld, J.B. Newman, The development and stability of surface layers on concrete exposed to sea-water, Cement Concr. Res. 16 (5) (1986) 721–732, https://doi.org/10.1016/0008-8846(86)90046-3.

[29] K. De Weerdt, H. Justnes, M.R. Geiker, Changes in the phase assemblage of concrete exposed to sea water, Cement Concr. Compos. 47 (2014) 53–63, https://doi.org/10.1016/j.cemconcomp.2013.09.015.

[30] H.F.W. Taylor, Cement Chemistry, second ed., Thomas Telford Publishing, London, 1997, pp. 259–260.

[31] K. De Weerdt, B. Lothenbach, M.R. Geiker, Comparing chloride ingress from seawater and NaCl solution in Portland cement mortar, Cement Concr. Res. 115 (2019) 80–89, https://doi.org/10.1016/j.cemconres.2018.09.014.

[32] M. Collepardi, A. Marcialis, R. Turriziani, The kinetics of chloride ions penetration in concrete, Il cemento 67 (1970) 157–164.

[33] L. Mejlbro, The complete solution of Fick's second law of diffusion with time-dependent diffusion coefficient and surface concentration, in: P. Sandberg (Ed.), Durability of Concrete in Saline Environment, Cementa AB, Lund, Sweden, 1996, pp. 127–158.

[34] A.J.M. Siemes, C. Edvardsen, T.N.O. Bouw, in: M.A. Lacasse, D.J. Vanier (Eds.), Duracrete: Service Life Design for Concrete Structures, NRC Research Press, Ottawa, Canada, 1999.

[35] S. Engelund, General Guidelines for Durability Design and Redesign: DuraCrete, Probabilistic Performance Based Durability Design of Concrete Structures [Gouda], [CUR], 2000.

[36] fib, Model code for service life design - bulletin 34, fédération internationale du béton (fib), 2006. Lausanne, Switzerland.

[37] L. Tang, L.-O. Nilsson, P.A.M. Basheer, Resistance of Concrete to Chloride Ingress: Testing and Modelling, first ed., Spon Press, London, 2012.

[38] Y. Hosokawa, K. Yamada, B.E. Johannesson, L.-O. Nilsson, Models for chloride ion bindings in hardened cement paste using thermodynamic equilibrium calculations, in: 2nd International RILEM Symposium on Advances in Concrete through Science and Engineering, Quebec City, Canada, 2006.

[39] M. Alexander, A. Bertron, N. De Belie, Performance of Cement-Based Materials in Aggressive Aqueous Environments, Springer, 2013.

[40] C. Andrade, M.A. Climent, G. De Vera, Procedure for calculating the chloride diffusion coefficient and surface concentration from a profile having a maximum beyond the concrete surface, Mater. Struct. 48 (4) (2015) 863–869, https://doi.org/10.1617/s11527-015-0543-4.

[41] F. Toutlemonde, C. Andrade, C.V. Nielsen, S. von Greve-Dierfeld, Draft of Background Document for prEN1992-1-1:2020 D7 Clause 6 - Durability, CEN/TC 250/SC 2/WG 1/TG 10, 2021.

[42] DS/EN 197-1, Cement - Part 1: Composition, Specifications and Conformity Criteria for Common Cements, 2011. Danish standard.

[43] DS/EN 196-2, Method of Testing Cement - Part 2: Chemical Analysis of Cement, Danish Standard, 2013.

[44] Fehmarnbelt Exposure Site, 2015. http://www.concreteexpertcentre.dk/30663, 15th of March 2021.

[45] A. Demayo, Elements in sea water, in: D.R. Lide (Ed.), CRC Handbook of Chemistry and Physics, CRC Press, USA, 1988.

[46] A.D. Herholdt, C.F.P. Justesen, P. Nepper-Christensen, A. Nielsen, Beton-Bogen, Cementfabrikkernes Tekniske Oplysningskontor, Aalborg Portland, Aalborg, Denmark, 1985.

[47] DS/EN 12390-1:2000, Testing Hardened Concrete - Part 1: Shape, Dimensions and Other Requirements for Specimens and Molds, Danish Standard, 2000.

[48] U. Jakobsen, P. Laugesen, N. Thaulow, Determination of Water-Cement Ratio in Hardened Concrete by Optical Fluorescence Microscopy, Special Publication, 1999, pp. 27–42, 191.

[49] DS/EN 12390-3 + AC:2012, Testing Hardened Concrete - Part 3: Compressive Strength of Test Specimens, Danish Standard, 2012.

[50] DS/EN 12390-7:2012, Testing Hardened Concrete - Part 7: Density of Hardened Concrete, Danish Standard, 2012.

[51] S. Fjendbo, H.E. Sørensen, K.d. Weerdt, M.R. Geiker, When and How Should Chloride Profiles Be Calibrated for Paste Fraction?, Manuscript submitted for publication 2021.

[52] B. Lothenbach, P. Durdzinski, K. De Weerdt, Thermogravimetric analysis, in: K. Scrivener, R. Snellings, B. Lothenbach (Eds.), A Practical Guide to Microstructural Analysis of Cementitious Materials, CRC Press, 2016, pp. 177–211.

[53] K. Scrivener, R. Snellings, B. Lothenbach, A Practical Guide to Microstructural Analysis of Cementitious Materials, CRC Press, 2018.

[54] E.J. Sellevold, T. Farstad, The PF-method–A simple way to estimate the w/c-ratio and air content of hardened concrete, in: Third International Conference on Construction Materials: Performance, Innovations and Structural Implications and Mindess Symposium, Vancouver, Canada, 2005.

[55] U.H. Jakobsen, N. Thaulow, Combining Optical Fluorescent Microscopy and Scanning Electron Microscopy for the Examination of Deteriorated Concrete, Procedings of 7th Euroseminar on Microscopy Applied to Building Materials, 1999. Delft, Netherlands.

[56] U. JACOBSEN, N. Thaulow, Sulphate attack as observed by optical and scanning electron microscopy, in: Cement and Concrete Technology in the 2000s, Procedings of Second International Symposium, 2000, pp. 6–10.

[57] K. De Weerdt, M.R. Geiker, D. Orsáková, Investigation of Concrete from Solsvik Field Station: 4 Concrete Cores Investigated after 16 Years of Submerged Exposure, Norwegian Public Roads Administration, 2015, p. 47.

[58] T.C. Powers, T.L. Brownyard, Studies of the Physical Properties of Hardened Portland Cement Paste, Portland Cement Association, 1948. Research Laboratories 43.

[59] G.W. Washa, K.F. Wendt, Fifty year properties of concrete, ACI Journal Proceedings 72 (1) (1975) 20–28.

[60] K. Walz, FESTIGKEITSENTWICKLUNG VON beton BIS zum alter VON 30 UND 50 JAHREN, in: K. Walz (Ed.), Betontechnische Berichte, Forschungsinstitut der Zementindustrie, 1976. Düsseldorf.

[61] M. Maage, S. Smeplass, R. Johansen, Long-term Strength of High-Strength Silica Fume Concrete, vol. 121, ACI Special Publication, 1990, pp. 399–408.

[62] H. Al-Khaiat, N. Fattuhi, Long-term strength development of concrete in arid conditions, Cement Concr. Compos. 23 (4–5) (2001) 363–373, https://doi.org/10.1016/S0958-9465(01)00004-X.

[63] P.-C. Aitcin, P. Laplante, Long-term compressive strength of silica-fume concrete, J. Mater. Civ. Eng. 2 (3) (1990) 164–170, https://doi.org/10.1061/(ASCE)0899-1561(1990)2:3(164).

[64] M.D. Thomas, P.B. Bamforth, Modelling chloride diffusion in concrete: effect of fly ash and slag, Cement Concr. Res. 29 (4) (1999) 487–495, https://doi.org/10.1016/S0008-8846(98)00192-6.

[65] T. Luping, I. Löfgren, Evaluation of Durability of Concrete with Mineral Additions with Regard to Chloride-Induced Corrosion, Department of Civil and Environmental Engineering, Chalmers University of Technology, 2016.

[66] T.U. Mohammed, H. Hamada, T. Yamaji, Concrete after 30 years of exposure—Part II: chloride ingress and corrosion of steel bars, Materials Journal 101 (1) (2004) 13–18.

[67] A. Machner, M. Zajac, M.B. Haha, K.O. Kjellsen, M.R. Geiker, K. De Weerdt, Stability of the hydrate phase assemblage in Portland composite cements containing dolomite and metakaolin after leaching, carbonation, and chloride exposure, Cement Concr. Compos. 89 (2018) 89–106, https://doi.org/10.1016/j.cemconcomp.2018.02.013.

[68] M. Frías, S. Goñi, R. García, R.V. de La Villa, Seawater effect on durability of ternary cements. Synergy of chloride and sulphate ions, Compos. B Eng. 46 (2013) 173–178, https://doi.org/10.1016/j.compositesb.2012.09.089.

[69] T. Cheewaket, C. Jaturapitakkul, W. Chalee, Long term performance of chloride binding capacity in fly ash concrete in a marine environment, Construct. Build. Mater. 24 (8) (2010) 1352–1357, https://doi.org/10.1016/j.conbuildmat.2009.12.039.

[70] M. Thomas, Supplementary Cementing Materials in Concrete, CRC press, 2013.

[71] J. Marchand, Modeling the behavior of unsaturated cement systems exposed to aggressive chemical environments, Mater. Struct. 34 (4) (2001) 195–200, https://doi.org/10.1007/BF02480588.

[72] Y. Elakneswaran, T. Ishida, Development of A Physical and Geochemical Model for Long-Term Performance of Cementitious Materials, Society for Social Management Systems Internet Journal, 2012.